RSC Applied Polymers

ROYAL SOCIETY OF CHEMISTRY

REVIEW

View Article Online
View Journal | View Issue

Cite this: *RSC Appl. Polym.*, 2024, **2**, 507

Polymer composites with 3D graphene architectures as high-performance EMI shielding materials: a review

Suman Chhetri *[a] and Tapas Kuila *[b,c]

Secondary electromagnetic pollution generated due to the inevitable reflection in solid/thin film conducting polymer composites has been a major barrier in realizing high-performance absorption-dominated electromagnetic interference (EMI) shielding. In the past, prodigious efforts were made to minimize the reflection by tailoring the impedance characteristics between the air and the substrate. For instance, incorporation of a microcellular scaffold (3D structure) such as foam and aerogel in a polymer matrix have been extensively investigated to tailor the surface impedance matching and achieve enhanced absorption. To date, application of the 3D graphene microcellular scaffold alone or its hybrid with other magnetic, conductive, and dielectric materials has been continuously pursued to diminish reflectivity and increase absorption *via* the dielectric and interfacial relaxation loss mechanism. An aerogel and foam structure contains multiscale pores (micro and nano scale pores). Through the large number of solid/air interfaces created by such pores, it can efficiently tune the impedance matching. The solid/air interface renders surplus EM wave attenuation capabilities by increasing the EM wave trajectory path *via* internal scattering within the pores. The 3D graphene architectures-based polymer composites show hitherto EMI shielding efficiency improvement at significantly low mass density and percolation threshold. However, most of the existing studies on 3D graphene-based composites rely on trial-and-error methods without comprehensively investigating the effect of the geometrical and microstructures aspects on the EMI shielding performance. Furthermore, the state-of-art literature does not (re)present an analytical/theoretical model that can be employed to optimize parameters appropriate for designing the absorption-dominated shielding material with diminished reflection. This review is intended to cover the latest progress and innovation around 3D graphene nanostructure-based polymer composites as EMI shielding materials. The EMI shielding properties of the composites, including graphene aerogels, foam and hybrid aerogel/foam, with other dielectric and magnetic materials are discussed along with the underlying mechanism. In addition, this review represents an input impedance model that can be utilized in conjunction with experimental design to optimize geometrical and microstructural parameters to realize an absorption-dominated shielding material. Based on the available status on 3D graphene scaffold-based composites, we summarize the current achievements and offer a route toward future developments.

Received 20th February 2024,
Accepted 16th April 2024

DOI: 10.1039/d4lp00061g

rsc.li/rscapplpolym

1. Introduction

Electronic pollution such as electromagnetic (EM) radiation emanating from various sources such as communication devices, integrated circuits, and high-power operating appliances is emerging as a global challenge. EM radiation emitted in the range of frequencies that meddles with the input signals of electronic devices creates interference known as electromagnetic interference (EMI), which is detrimental to the operation of sensitive equipment.[1–7] EMI is a disturbance where the electromagnetic field generated by one component interferes with another, leading to degradation and malfunctioning of sensitive electronic devices.[8,9] This is why people are asked to switch off their mobile phones while boarding aircraft, fearing that it may cause failure of sensitive components or disruption of the communication signal with the air traffic control. EMI is not only fatal to sensitive electronic components but also has severe implications on human health and environment.[10,11] The EM energy could proliferate into body cells, leading to body temperature elevation and dis-

[a]*Department of Mechanical Engineering, College of Engineering, University of Hawaii at Manoa, Honolulu, 96822, USA. E-mail: chhetri@hawaii.edu, chhetrisuman86@gmail.com; Tel: +1-808-8078-144*
[b]*Electric Mobility & Tribology Research Group, Council of Scientific and Industrial Research-Central Mechanical Engineering Research Institute, Durgapur, 713209, India. E-mail: tkuila@gmail.com*
[c]*Academy of Scientific and Innovative Research (AcSIR), CSIR-Human Resource Development Centre, (CSIR-HRDC) Campus, Postal Staff College Area, Sector 19, Kamla Nehru Nagar, Ghaziabad, 201002 Uttar Pradesh, India*

abling protein function. Beside the hazards to the human health and environment, the EM pollution is equally damaging to agricultural fields, ruining the growth of crops and turning fertile growing fields into barren land. Thus, to confront the rapidly increasing electromagnetic pollution and to minimize EMI, the need to develop high-performance shielding materials has become inevitable, mainly for sensitive equipment. The shielding material basically acts as an enclosure to cut off the interaction of the sensitive components with the external environment, so that the penetrating radiation is abated before reaching the interior circuit. This is achieved by reflecting or absorbing the EM wave. Metal and metal-based composites are generally preferred as shielding materials on account of their superior conductivity, magnetic permeability, and wide bandwidth.[12] However, the electrical conductivity-dependent shielding effectiveness in metals-based thin films inevitably usher the generation of secondary pollution due to the strong surface reflection. Furthermore, the high propensity of metal toward corrosion, difficulties in processing and mounting on a complex structure, and density issues have also made metal-based materials incompatible with the evolving technology.[13,14] All of these imperfections have paved the way for polymer composites-based shielding materials in this realm. Although a few attributes make the polymer system a suitable EMI shield against the metal-based shielding material, the majority of the polymers are insulating to the EM wave, which precludes its direct application. Thus, conducting fillers such as carbon black, carbon nanofibers, carbon nanotubes, and graphene have evoked wide attraction as potential reinforcing components.[15–20]

Among the conductive fillers mentioned above, the lowest electrical percolation threshold has been achieved with graphene, which is attributed to its high specific surface area, tunable electrical properties, and potentially connecting sheets.[21,22] Achieving the targeted EMI shielding value at a lower percolation threshold is a significant advantage, as it reduces costs and the density of the composite material. In this regard, graphene, on account of its outstanding structure and characteristics, has been widely pursued in developing EMI shielding polymer composites.[22,23] Reduced graphene oxide (rGO), a derivative of graphene that is mainly employed in developing composites, is considered a promising candidate due to its controllable dielectric loss that stems from residual functional groups and defects, which promote dielectric loss through defect polarization and dipole relaxation.[24] Furthermore, the functional groups on its surface are conducive to anchoring other dielectric and magnetic materials, efficiently increasing the EM loss ability of the material and enabling the tailoring of impedance matching as well. Integrating the graphene/derivative of graphene with the polymer renders the seminal EMI shielding effectiveness (EMI SE) through electric and conduction loss.[25] The EMI shielding performance of composites incorporating conductive fillers, whether in film or solid material form, mostly relies on conductivity. The high electrical conductivity of the filler network can cause an impedance mismatch between the shield and the air, enhancing the reflection and giving rise to secondary pollution.[26–28] To circumvent secondary pollution, absorption-dominated materials are gaining attention as an EMI shield, where the EM wave absorption/reflection (A/R) ratio is expected to be greater than 1.[29,30] A larger A/R ratio corresponds to less reflection, where the majority of incident waves are attenuated by the material through dielectric or magnetic loss. The integration of a microcellular 3D scaffold (foam, aerogel, sponge)

Suman Chhetri

Dr Suman Chhetri is currently a postdoctoral associate in the Department of Mechanical Engineering at the University of Hawaii at Manoa, working with Prof. Woochul Lee on solar-driven desalination, polymer nanocomposites, phase change materials, and electrocatalysts. He received his Ph.D. in Chemical Science from AcSIR – Academy of Scientific & Innovative Research, India, in 2019. His Ph.D. research focused on developing, characterizing, and applying functionalized graphene-based epoxy nanocomposites. The study included evaluations of thermal, mechanical, EMI shielding, and anti-corrosion properties.

Tapas Kuila

Dr Tapas Kuila has been working as a Principal Scientist at CSIR-Central Mechanical Engineering Research Institute, Durgapur, India. He joined this Institute in 2012 as a DST Inspire Faculty Fellow, and joined as a Senior Scientist in November, 2017. Dr Kuila completed his Ph.D. study in Chemistry from Indian Institute of Technology, Kharagpur, in 2009. Then, he moved to Jeonbuk National University, South Korea, for his postdoctoral study. Dr Kuila has been working in the areas of graphene ultracapacitors, hydrogen storage, graphene/epoxy composites, graphene lubricants, piezoelectric sensors and graphene enhanced phase change materials. He has published ~160 research/review articles in different international peer-reviewed journals. Dr Kuila has also authored 20 book chapters and 2 Indian patents.

with the polymer matrix has been considered a promising way to tailor the impedance matching and diminish the EM wave reflectivity.[26,31] In this regard, the 3D graphene microcellular scaffold alone or its hybrid with magnetic, conductive, and other dielectric materials has been continuously pursued to enhance absorption through the interfacial and dipole polarisation loss mechanism.[32,33] The 3D graphene-based architectures represent a highly interconnected micro/macroporous structure possessing ultra-low-density characteristics, and a high surface area with advantages of efficient flow of charge and ion.[34] The 3D network in aerogels and foams reduces the buildup of conductive particles in the cell wall and yields an appropriate pore structure. Within this structure, trapped air optimizes impedance matching, thereby reducing reflection and enhancing absorption.[35,36] Moreover, the structure of aerogels and foams contains multiscale pores (micro and nano-scale pores). Through the large number of solid/air interfaces created by these pores, they efficiently tune impedance matching. This interface provides surplus EM wave attenuation capabilities by increasing the EM wave path through internal scattering within the pores.[6] Furthermore, the design of a 3D scaffold can assist with the uniform dispersion of filler, enabling the formation of a connected electrical network for efficient electron flow, thereby achieving superior shielding performance at lower filler loading. When it comes to nanofillers, regardless of their types, preventing their inevitable agglomeration within the polymer matrix is crucial to realizing their true potential.

To date, numerous studies on 3D graphene-based polymer composites have been reported, showing encouraging shielding effectiveness based on absorption-dominated mechanisms. However, there is a lack of studies focused on deciphering the significance of structural and geometrical factors in developing absorption-dominated shielding materials.[32,37,38] For example, the scaffold thickness (geometry) and morphology (microstructure) can be a crucial variable affecting the surface impedance matching and reflectivity, the optimization of which can lead to high performance absorption-dominated shielding materials.[39,40] However, most of the current studies have been executed on trial-and-error methods, hardly exploring the actual shielding mechanism governing the structure-EMI shielding performance of these class of materials. Studying the relationship between the thickness of the 3D scaffold, pore structure and corresponding shielding performance is crucial to obtaining an optimized reflectivity and A/R ratio critical for the absorption-dominant shielding material. In addition, there is a lack of analytical formulation-based approaches to provide direction and guidelines for modulating the structural design of absorption-dominated EMI shielding in 3D graphene architecture-based polymer composites, aiming to reduce reflection and achieve a high A/R ratio. Comprehensive review articles emphasizing analytical approaches that could save researchers' resources and time in designing high-performance shielding materials are not readily available. Also, analytical formulation is crucial to understanding the underlying mechanism central to the structure-shielding properties. The effect of structural and geometrical factors on the optimal reflectivity and A/R ratio must be quantitatively studied to design an EMI shielding material with optimized absorption-dominant performance. This review article intends to cover the recent development of 3D graphene-based microstructure (GA and GF, along with hybrid multi-phase heterostructure) polymer composites in the realm of EMI shielding application, and represents an analytical approach that could be useful to optimize the geometrical and structural factors that are decisive toward achieving absorption-dominated 3D graphene-based polymer composites with reduced reflectivity. The represented input impedance model can be used to quantitatively assess the thickness dependence of the EM wave reflectivity, and provide guidelines for designing monolayer and gradient-layered structures consisting of 3D graphene and polymer with tailored impedance suitable for realizing an absorption-dominant mechanism. Fig. 1 schematically represents the EM radiation propagation and scattering across 3D graphene scaffold-based polymer composites. The current state-of-the-art, accomplished milestones, challenges, and future directions in this area have been discussed thoroughly.

2. EMI shielding model based on transmission line theory and wave equations

EMI shielding is a barrier employed between the wave emitter and the receptor to diminish the coupling of unwanted radiation. Let us consider a uniform plane wave encompassing electric field E and magnetic field H. Based on the transmission line theory, Maxwell's equation can be expressed as;[41–43]

$$\frac{dE}{dx} = -j\omega\mu H = \hat{y}E \quad (1)$$

$$\frac{dH}{dx} = -(\sigma + j\omega\varepsilon)E = \hat{z}H \quad (2)$$

In the above equation, $\hat{y}$ and $\hat{z}$ denote the admittivity and impedivity of the medium, respectively. μ is the permeability of the material, which can be written as $\mu = \mu_0\mu_r$. μ_0 is the absolute permeability of air (1.268×10^{-6} H m^{-1}), and μ_r is the relative complex permeability (material to air, $\mu_r = \mu' - j\mu''$). σ is

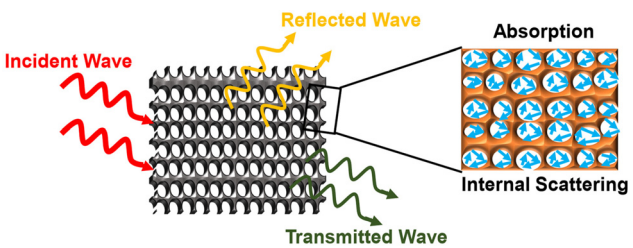

Fig. 1 Schematic showing a propagation of the EM radiation, scattering and absorption in a 3D graphene-scaffold.

the conductivity of the material. ε is the permittivity of the material, and can be represented as $\varepsilon = \varepsilon_0\varepsilon_r$. ε_0 is the absolute permittivity of the air (8.85×10^{-12} F m^{-1}), and ε_r is the relative complex permittivity ($\varepsilon_r = \varepsilon' - j\varepsilon''$). ω is angular frequency and can be written as $\omega = 2\pi f$. Based on the wave eqn (1) and (2), the variations of the electric field along the thickness direction of the medium can be depicted by the propagation constant ($\gamma = \sqrt{\hat{y}\hat{z}}$) :[40,42]

$$E = E_i e^{-\gamma t} \tag{3}$$

where E is the electric field at a distance "t".

$$\gamma = \sqrt{\hat{y}\hat{z}} = \gamma = \sqrt{j\omega\mu(\sigma + \omega\mu)} = \alpha + j\beta \tag{4}$$

Here, α is the attenuation constant and β is the phase constant. The attenuation constant, α, can be written as function of ω, μ, σ and ε of the shield based on eqn (5).

$$\alpha = \omega\sqrt{\frac{\mu\varepsilon}{2}}\left(\sqrt{1 + \left(\frac{\sigma}{\omega\varepsilon}\right)^2} - 1\right) \tag{5}$$

All homogenous materials are described by the intrinsic impedance, which is the ratio of E to H as represented in eqn (6), and transmission line theory requires the continuity of the input and output intrinsic impedance of the two media, or a reflection of the EM will occur.[42]

$$\eta = \sqrt{\frac{\hat{z}}{\hat{y}}} = \sqrt{\frac{j\omega\mu}{(\sigma + j\omega\varepsilon)}} \tag{6}$$

For a dielectric material, $\sigma \ll \omega\varepsilon$; hence, the impedance from eqn (6) can be written as:

$$\eta = \sqrt{\frac{\mu}{\varepsilon}} \tag{6a}$$

For a conducting material, $\sigma \gg \omega\varepsilon$; thus, the impedance from eqn (6) can be written as:

$$\eta = \sqrt{\frac{j\omega\mu}{\sigma}} \tag{6b}$$

The impedance of an EM wave is defined by the tangential component of the electric field, E, and magnetic field, H, $Z = \frac{|E|}{|H|}$. For a homogenous layer of thickness t, the impedance can be expressed as below:[39,43,44]

$$Z = \eta\frac{Z(t)\cosh\gamma t + \eta\sinh\gamma t}{\eta\cosh\gamma t + Z(t)\sinh\gamma t} \tag{7}$$

In the above equation, $Z(t)$ is the impedance at interface t. Notably, a reflection will occur if $Z(t) \neq \eta$.

The total shielding effectiveness (SE) is defined by:

$$SE = -20\log_{10}|T| \tag{8}$$

The total shielding effectiveness comprises the absorption $\alpha_A = 20\log_{10}|e^{-\gamma t}|$, the reflection $\alpha_R = 20\log_{10}|p|$, and the successive internal reflection $\alpha_B = 20\log_{10}|1 - qe^{-2\gamma t}|$, where p and q are the transmission and reflection coefficients, respectively, and the value of T is written as;

$$T = p(1 - qe^{-2\gamma t})^{-1}e^{-\gamma t}$$

Based on transmission line theory,[45–47] the interaction between a propagating EM wave and EMI shielding material can be thought of as a circuit in the transmission line. Thus, layered materials with i numbers of layers can be modelled as multiple impedance components connected in series. A multilayer EMI shielding material with i layers can be considered to have $i + 1$ impedance sections in series in the circuit. Here, air serves as a substrate and hence considered as one impedance section in the circuit. In this situation, the perforating EM wave will undergo a reflection at each interface between all bordering impedance components. Therefore, the total reflectance (R) corresponding to the layered shielding material can be represented by a function of the output impedance (z_{out}) and input impedance (z_{in}):[39,48,49]

$$R = \left(\frac{z_{in} - z_{out}}{z_{in} + z_{out}}\right)^2 \tag{9}$$

where z_{out} is the intrinsic impedance of air ($z_{out} = \eta_0 = 377\ \Omega$).

As it is discussed, the reflection not only happens at the surface of the shield, but it also will occur between all adjoining sections with different impedances in the circuit. Thus, the surface input impedance for an EMI shield can be expressed as a function of the intrinsic impedance of the layer in consideration (η_i), propagation constant, γ_i, thickness (t_i) of the layer in consideration (i^{th} layer, surface layer), and the input impedance of subsequent sections (z_{i-1}, surface impedance of the $i - 1^{st}$ layer), which can be represented as:[39,43,44]

$$\begin{aligned} z_{in} = \left|\frac{E}{H}\right| &= \eta_i\frac{z_{i-1}\cosh(\gamma_i t_i) + \eta_i\sinh(\gamma_i t_i)}{\eta_i\cosh(\gamma_i t_i) + z_{i-1}\sinh(\gamma_i d_i)} \\ &= \eta_i\frac{z_{i-1} + \eta_i\tanh(\gamma_i t_i)}{\eta_i + z_{i-1}\tanh(\gamma_i t_i)} \end{aligned} \tag{10}$$

Then, the absorption of the i layers is written as:

$$\alpha_A = 20\log_{10}|e^{\gamma_0 t_0 + \gamma_1 t_1 + \cdots\gamma_i t_i}| \tag{11}$$

The total reflection can be depicted as the sum of the reflection at each boundary (interface),

$$\alpha_R = 20\log_{10}\left|\frac{1}{2^i}\left(1 + \frac{\eta_0}{Z_\omega}\right)\left(\frac{\eta_1}{\eta_0}\right)\ldots\left(1 + \frac{Z_\omega}{\eta_i}\right)\right| \tag{12}$$

and the consecutive internal re-flection is expressed as:

$$\alpha_B = 20\log_{10}|(1 - q_0e^{-2\gamma_0 t_0})(1 - q_1e^{-2\gamma_1 t_1})\ldots(1 - q_ie^{-2\gamma_i t_i})| \tag{13}$$

where Z_ω is the impedance of the incident wave.

As can be seen in eqn (11), the absorption is related to the propagation constant γ_i to $\sigma_i\mu_i$ as eqn (4), and to the film thickness, t_i. According to eqn (12), the reflection does not depend on the thickness. However, it is characterized by the impedance ratio of the bordering layers. The internal re-reflection, akin to absorption, is also a function of the layer thickness. The impact of the reflection to the shielding effectiveness

becomes more significant as the number of layers increases. The reflection mechanism at the interface between the two layers becomes critical and governs the shielding effectiveness. As absorption-dominated materials are becoming crucial to circumvent the effect of secondary pollution, theoretical models to guide the design and fabrication of optimal EM wave reflection shielding materials are paramount to address this issue. An input impedance model can be employed to reveal the effect of the microstructure (*e.g.*, void fraction, pore size, cellular morphology) and structural (thickness) factor of each layer on the impedance matching and reflectivity of the layered foam/aerogel composites. This analytical model can guide the optimization of the structural and microstructural parameters of each layer to realize suitable input impedance matching and achieve an absorption-dominated shielding mechanism with reduced reflection.

The intrinsic impedance of the i^{th} layer can be written as

$$\eta_i = \sqrt{\frac{j\omega\mu_i}{\sigma_i + j\omega\varepsilon_i}} = \eta_0\sqrt{\frac{\mu_{ri}}{(\varepsilon_{ri} + \sigma/j\omega\varepsilon_0)}} \quad (14)$$

and the propagation constant of the i^{th} layer can be expressed as

$$\gamma_i = \sqrt{j\omega\mu_i(\sigma_i + j\omega\varepsilon_i)} = j\frac{\omega}{c}\sqrt{\mu_{ri}\left(\varepsilon_{ri} + \frac{\sigma_i}{j\omega\varepsilon_0}\right)} \quad (15)$$

where c is the speed of light, and μ_i, ε_i and σ_i represent the permeability, permittivity, and conductivity of the i^{th} layer, respectively.

It should be noted that, in most studies associated with semi-conductive materials, the σ term is neglected from the impedance equation as $\sigma \ll \omega\varepsilon$. However, such practice in the case of conductive polymer composites with an electrical conductivity of more than 1 S m^{-1} may lead to an error that cannot be ignored. For 3D graphene (aerogel, hydrogel) polymer composites, two impedance components (composites and air substrate) must be considered in a circuit. Using eqn (7, 10, 14) and (15), the input impedance for a monolayer polymer composite shielding material can be represented as:

$$Z_{in} = \eta_0\sqrt{\frac{\mu_r}{(\varepsilon_r + \sigma/j\omega\varepsilon_0)}}\frac{1 + \sqrt{\frac{\mu_r}{(\varepsilon_r + \sigma/j\omega\varepsilon_0)}}\tanh\left(j\omega/c\sqrt{\mu_r\left(\varepsilon_r + \frac{\sigma}{j\omega\varepsilon_0}\right)}t\right)}{\tanh\left(j\omega/c\sqrt{\mu_r\left(\varepsilon_r + \frac{\sigma}{j\omega\varepsilon_0}\right)}t\right) + \sqrt{\frac{\mu_r}{(\varepsilon_r + \sigma/j\omega\varepsilon_0)}}} \quad (16)$$

As mentioned above, in EMI shielding materials, air serves as a substrate; hence, $Z_{out} = Z_0 = 1$. The R value of the material can then be defined as

$$R = \left(\frac{z_{in} - 1}{z_{in} + 1}\right)^2 \quad (17)$$

As per eqn (14) and (16), if the relative complex permeability, thickness, conductivity, and relative complex permittivity are known, the dependence of the reflectivity R on the thickness of each layer can be calculated, and this method is termed as the input impedance based on transmission line theory. This method can be employed to design multilayered shielding materials based on 3D graphene-based polymer composites with diminished reflectivity. The equations indicate that the scaffold thickness plays a crucial role in tuning the surface impedance matching conditions, and in realizing the diminished reflection for absorption-dominated EMI shielding. Furthermore, eqn (14)–(16) can be utilized to calculate the reflectivity of composites containing a 3D scaffold with varying cell sizes (pore sizes), volume fractions, and other parameters. The electrical properties and impedance characteristics of the 3D scaffold can be essentially adjusted by changing the pore sizes and volume fractions, which, in turn, can either increase or decrease the secondary reflection. The effective EM wave absorption ability of the 3D scaffold generally depends on their conductive network optimization and bulk density adjustment.[50] The density of the scaffold can be altered by changing the pore size, while keeping the volume fraction constant. A scaffold with small pore sizes forms discontinuous cell walls, leading to fewer electrically conductive pathways. Conversely, a scaffold with large pore sizes forms an interconnected network, resulting in numerous conductive paths. Furthermore, the number of contact junctions in large pore size scaffolds is comparatively small, resulting in a diminished contact resistance due to the effective overlapping region. Wan *et al.* prepared graphene aerogels with different pore sizes, and observed that the scaffold with larger pore sizes exhibited higher electrical conductivity.[51] This was attributed to a seamless interconnected network that enabled effective and rapid channels for electron transport, in contrast to the scaffold with smaller pore sizes. The decrease in electrical conductivity is beneficial for surface impedance matching, which in turn results in a reduced reflection of the EM waves. The EMI shielding performance of epoxy composites developed with the large pore size graphene aerogel was found to be higher than that of composites containing a small pore size scaffold. It should be noted that a decrease in the electrical conductivity often leads to a reduction in the EMI shielding efficiency, as the attenuation constant (eqn (5)) and permittivity are directly linked to the electrical conductivity. However, a recent study has shown that the absorption capability *via* dielectric loss in small pore size scaffolds compensates for the reduction in the electrical conductivity.[39] Therefore, the model presented above can also be used to design scaffolds with optimum density and microstructure that attenuate maximum EM waves and reflect minimally.

3. Preparation of 3D graphene architectures

Widely explored 3D graphene-based architectures can be categorized into gels and foams; the gels include aerogels and hydrogels. Generally, the production technique of 3D graphene architectures includes assembly *via* physical/chemical inter-

actions, template methods, electrochemical reduction, controlled filtration, sol–gel synthesis and chemical foaming method.[52–60] The micro/nano structure (pore size, density, pore volume) of the 3D graphene scaffold depends upon the method followed to prepare these structures, and it endows both advantages and disadvantages to its properties. Moreover, the micro-structure can be tuned by varying the concentration of the precursor, the temperature, and by regulating the compression strain. The 3D graphene scaffold offers a huge prospect to enhance the EM wave absorption performance by tailoring the porous structure and microstructure for better impedance matching. Fig. 2 shows the 3D graphene architecture fabricated by different methods. Fig. 2a shows the CVD growth of GF and latterly compressed GF (cGF), where the laterally compressed Ni foam was employed to grow cGF. Fig. 2b depicts the graphene aerogel that was prepared following the self-assembly reduction process. A graphene aerogel with a different microstructure could be seen in the schematic resulting from a different-sized GO precursor. Fig. 2c & d represents the 3D rGO-GNF scaffold prepared by bubble template, and the Ag/GO foam achieved from assembling followed by freeze-drying.

3.1 Self-assembly through chemical cross-linking

GO, having pool of oxygen functional groups, can be conveniently used as a basic starting material to construct a 3D framework *via* chemical cross-linking. As this process involves the creation of a chemical bond between the GO sheets, the so-formed 3D scaffold is relatively stable and more robust than those achieved by other methods. La^{3+} or polyethylene imine have been employed as a cross-linking agent to fabricate graphene aerogels.[61] The unique strategy to promote edge-to-edge crosslinked GO sheets resulted in a mechanically robust aerogel with an ultrahigh surface area (up to 850 m^2). Although this strategy produces stable and strong aerogels, the extra step of reduction and freeze-drying process makes it lengthy and tedious.

3.2 Self-assembly through hydrothermal/solvothermal reaction

The self-assembly of GO through the hydrothermal/solvothermal reaction is the most followed approach to prepare graphene aerogels (GA)/graphene foam (GF), on account of the simplicity, prospect to control the reaction parameters, and the products formed with high purity and porosity.[62] The process is carried out by preparing the suspension of GO and sealed in a reactor, which is kept at high temperature for several hours, followed by freeze-drying and annealing to achieve GF. It is possible to control the macroscopic and microscopic attributes of a structure by controlling the hydrothermal duration, concentration of the GO suspension, and the pH of the precursor. By tailoring the above-mentioned parameters, the conductive network and dielectric attributes can be precisely controlled to balance the impedance match-

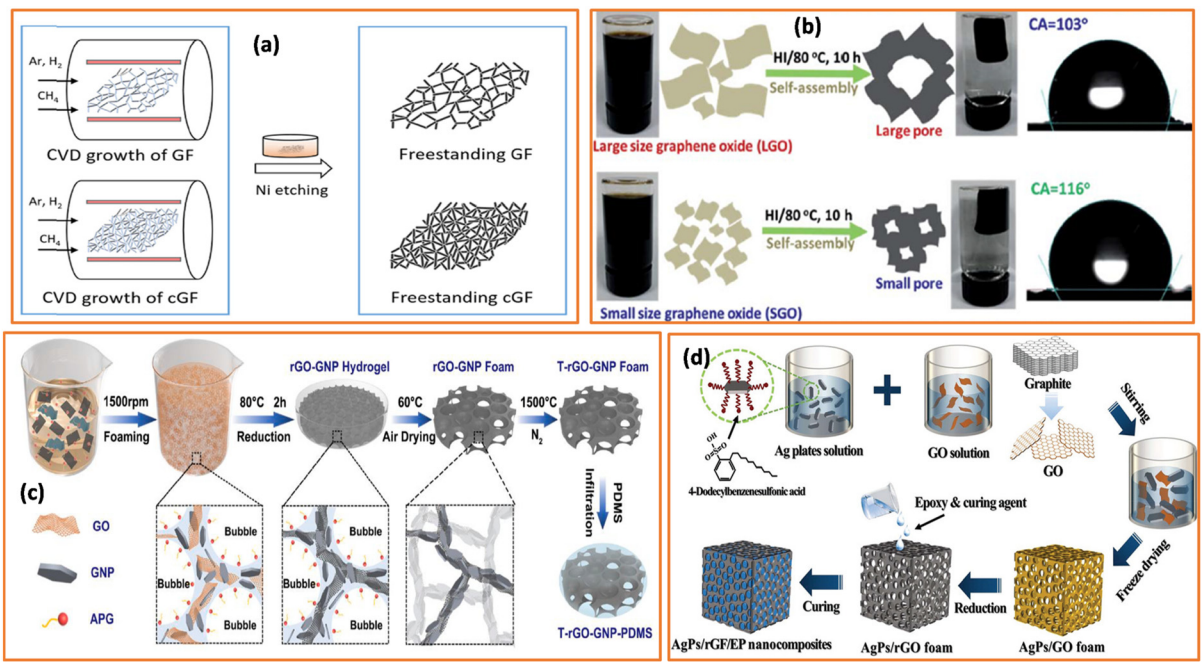

Fig. 2 Preparation of the 3D graphene scaffold following different methods. (a) Fabrication of the free-standing GF through chemical vapor deposition (CVD) using Ni as the template, reproduced with permission from ref. 32, copyright reserved Elsevier 2020. (b) Preparation of the varied cellular structure GA employing GO precursors of different sizes by self-assembly, reproduced with permission from ref. 51, copyright reserved Royal Society of Chemistry 2016. (c) Fabrication of the rGO-GNF foam following the bubble template method, reproduced with permission from ref. 85, copyright reserved Elsevier 2021. (d) Schematic for the preparation of the Ag/GO foam by assembling and freeze-drying of the functionalized silver platelets and GO, reproduced with permission from ref. 92, copyright reserved Royal Society of Chemistry 2019.

ing and attenuation capability. For instance, Wan *et al.* studied the effect of hydrothermal duration on the morphology of the graphene aerogel, and found that a short hydrothermal duration (4 h) failed to form strong interactions between the sheets. Conversely, a long hydrothermal duration (12 h) was able to produce a well-connected graphene skeleton with improved electrical conductivity and mechanical properties.[51] As the reaction is carried out at high temperatures and the GO sheets possess –COOH and –OH groups, an esterification reaction between the groups could crosslink the GO sheets, leading to 3D scaffold formation. However, the conventional hydrothermal approach suffers from a significant volume shrinkage of the precursor. Furthermore, the harsh environment employed during the preparation of GA through hydrothermal treatment restricts its acceptance to some degree. However, it is still a widely followed method. The engineering of the graphene surface prior to the hydrothermal treatment could be a possible way to overcome the issue associated with volume shrinkage. It should be noted that the structure formed might be loose and fragile as the self-assembly process involves a drying and dehydrating process, which is likely to weaken the interaction. To strengthen the interactions and confer mechanical stability to the fragile 3D graphene structure, a chemical cross-linker can be employed.

3.3 Self-assembly *via* chemical reduction

Although the hydrothermal self-assembly method has the potential to create a well-connected 3D graphene scaffold, the high temperature and long reaction duration limit its wide applications. Chemical reduction is another benign strategy to prepare GA under lower temperature, wherein a reducing agent is employed to self-assemble graphene sheets. It is worth noting that the self-assembly of reduced graphene sheets can be controlled by varying the mass ratios of the reducing agent and the precursor. Reducing agents, such as ammonia, hydrogen iodide (HI), hydrazine hydrate (N_2H_4), ethylenediamine (EDA), and Vitamin C, are the common chemicals used to reduce and assemble GO sheets. The GO solution under moderate temperature undergoes reduction, where oxygen-containing functional groups are diminished and the π conjugation in the carbon rings gets restored, resulting in reduced GO (rGO). As the π bonds are restored, the rGO sheets start restacking, forming aggregates and eventually turning to the 3D scaffold. This method can be used to design scaffolds with different pore sizes using different sized GO precursors. Wan *et al.* fabricated a graphene aerogel with tunable morphology and structure employing GO sheets with different sizes.[51] The extent of reduction is considered as a crucial parameter during the self-assembly, which depends on the duration of the reaction, the temperature, and the concentration of the reducing agent. The 3D graphene hydrogel has been fabricated using vitamin C as a reducing agent in 1 h only, which is much lower than the usual hydrothermal duration.[63] Although solution-based reduction offers the advantages of functionalization of the graphene surface and scaling up the process, the complex synthesis route and the complicated set-up limit its wide acceptance. Furthermore, the inevitable defects introduced during the breaking and making of bonds is detrimental to the charge flow.

3.4 Ice template method

The ice template method is one of the widely followed approaches to fabricate graphene aerogels, particularly the bidirectional freezing technique. This technique has been exploited to fabricate a long-range aligned lamellar 3D structure.[37] In the bidirectional freezing approach, the ice crystals act as templates for the ensuing 3D scaffold. The method includes the filling of the GO solution into a mould on a cold copper plate with an appropriate wedger as a spacer. While cooling down the plate, the wedger assists in generating both vertical and horizontal temperature gradients.[23] The ice crystals grow into a biaxially lamellar pattern, and the GO sheets assemble to duplicate the ice morphology. The basic idea is as follows: first, the GO suspension is frozen; second, the ice in the GO hydrogel is sublimated by freeze-drying to fabricate the 3D aerogel.[64,65] It is worth noting that the final structure of the scaffold (microstructure, porosity, orientation) and the ice nucleation and growth process can be tailored by parameters, such as the GO concentration, slope angle of the wedge, and the cooling rate. For instance, highly anisotropic graphene aerogels have been reported by the calcium ion-assisted unidirectional freezing of aqueous suspensions of GO, followed by freeze-drying and thermal reduction.[66] The so-formed graphene aerogel showed a highly oriented structure with graphene sheets arranged in a configuration parallel to the transverse direction. A nacre-mimetic 3D graphene architecture with a biaxial lamellar structure (fabricated through bidirectional freezing technique, followed by thermal reduction) has been infiltrated by a PDMS polymer to develop high-performance EMI shield composites.[37] Fig. 3a–d shows the schematic depicting the fabrication of the graphene aerogel with a lamellar structure and its composites with PDMS. Although the ice template method allows for the tuning of the 3D graphene architecture, the weak interactions between the graphene sheets due to sparse connections lead to weak mechanical strength and lower electrical conductivity.

3.5 CVD method

Alternatively, 3D structures with controlled morphologies and properties can be achieved by the direct growth of graphene on 3D templates using CVD methods, which is referred to as template synthesis. By using commercially available Ni foam, the 3D graphene structure has been directly grown, where the Ni foam acts as a template and catalyst.[52] The 3D template route is more viable than the conventional CVD process. In those respects, it could produce the prospective 3D structure in larger quantity, which benefits the applications where a huge amount of scaffold is required. In this process, Ni or Cu foam is used as a pattern for graphene foam growth. The merits of this method are a controllable number of graphene layers, size, and the quality of the scaffold, along with the adjustment prospect by changing the carbon source and template. The so-

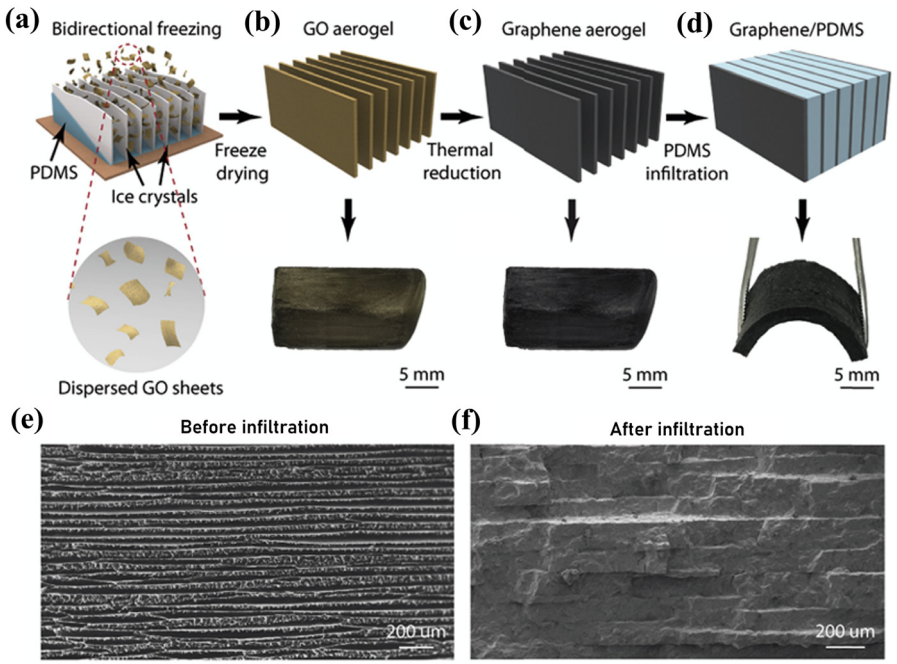

Fig. 3 Schematic depiction of the fabrication process of the anisotropic graphene/PDMS composite. (a) GO aerogels fabricated by bidirectional freeze casting technique. (b) GO aerogels with a lamellar structure formed after low temperature freezing dry at 10 Pa. (c) Graphene aerogels achieved by further thermal reduction of the GO aerogel. (d) Graphene/PDMS composites obtained by infiltrating PDMS into the graphene aerogel, and (e&f) GO aerogel before and after PDMS infiltration, reproduced with permission from ref. 37, copyright reserved Elsevier 2019.

formed interconnected network with high specific area and conductivity exhibits high porosity, and facilitates the smooth dispersion in the polymer composites. The porosity of GF achieved by this technique has been found to be as high as 99.7% and density as ~5 mg cm^{-3}.[67] GF obtained by CVD growth has been found to have lower boundary resistance against the GF prepared from the self-assembly process, which enables the electrons to move in the sheets with minimum hinderance. In addition, the CVD process does not introduce oxygen functionalities on the graphene surface, which leads to fewer defects and higher electrical conductivity. Although this technique produced the highest purity 3D graphene, the high temperature and the requirement of extra substrate as the template are obvious drawbacks. Fabrication of the 3D rGO-GNF scaffold was achieved following the bubble template method and the corresponding PDMS composite. The preparation of the fabrication of the 3D AgPs/rGF was achieved by freeze-drying treatment of GO and Ag.

4. Preparation of 3D graphene-based/polymer composites

4.1 Dip coating approach

The dip coating processing technique involves the immersion of the 3D graphene scaffold in the liquid polymer, and the parameters are varied to achieve the high-quality coating and composites. The parameters that influence the formation of high-quality composites are immersion or dipping time and the GF or GAs content. Coatings of various thicknesses can be achieved by varying the dipping time. After the formation of the coating, the system (composite) is allowed to cure at a certain temperature for a specific time. Fig. 4a depicts the fabrication of the GF/epoxy composites by the dip coating approach, where the 3D architecture is dipped into the liquid polymer to allow the coating process to take place on the porous scaffold.

4.2 Vacuum-assisted infiltration technique

The vacuum-assisted infiltration method has been a preferred technique to fabricate the 3D graphene-based epoxy or PDMS composite. To facilitate the infiltration, a polymer solution is first prepared in an appropriate solvent. Afterward, the 3D structure is immersed in the solution under vacuum to ensure smooth penetration into the scaffold pores and to remove trapped air bubbles. After completion of the infusion process, the wetted structure is removed from the solution and placed under vacuum at a certain temperature for solidification and to remove the solvent. Fig. 4b shows the fabrication of GA/epoxy composites using a vacuum-assisted infiltration technique, where the polymer solution infiltrates through the micro-pores of GA.[68] The polymer solution was heated to ensure the smooth penetration into the GA scaffold. The graphene content can be quantified by physically weighing the 3D structure before and after the infiltration process.

4.3 Template method

Here, the prepared 3D structure acts as a template framework wherein the polymer is backfilled. This fabrication technique

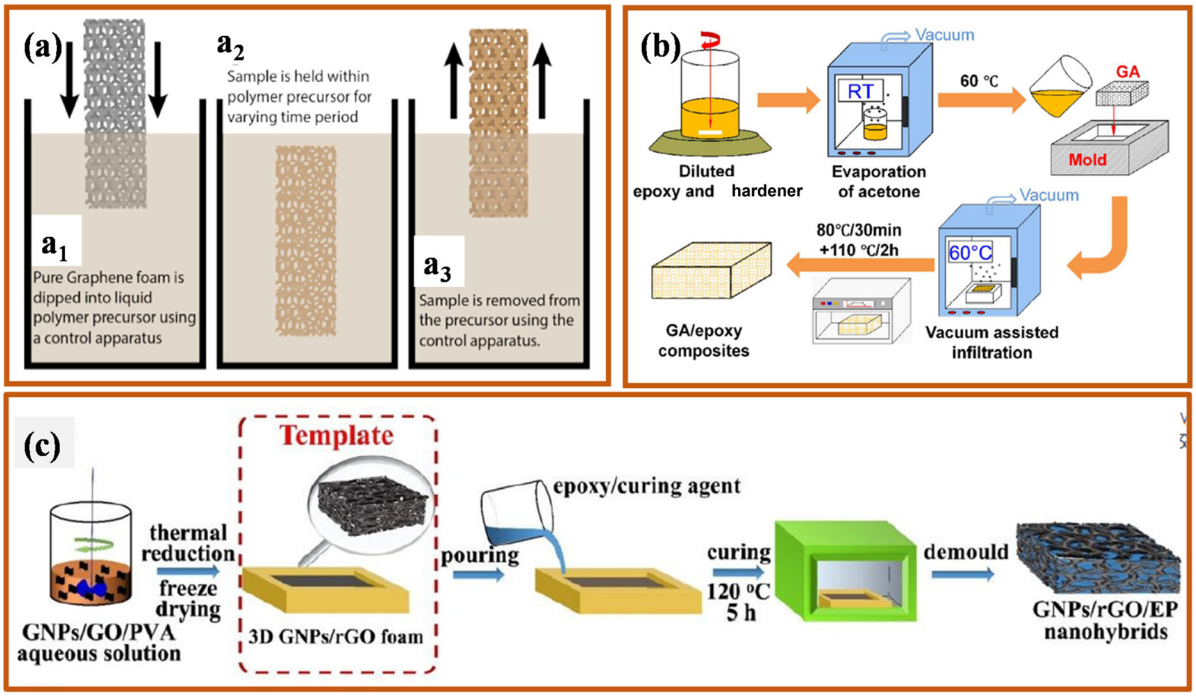

Fig. 4 Different fabrication processes of 3D graphene/polymer composites. (a) Schematic representation of the dip coating technique: (a_1) graphene foam was dipped, (a_2) held in the epoxy, and (a_3) retracted from the epoxy resin, followed by room temperature curing, reproduced with permission from ref. 34, copyright reserved Elsevier 2018. (b) Schematic illustration of the fabrication process of GA/epoxy composites following the vacuum-assisted infiltration technique, reproduced with permission from ref. 68, copyright reserved American Chemical Society 2015. (c) Depiction of the fabrication of GNPs/rGO foam/epoxy composites by template method, reproduced with permission from ref. 83, copyright reserved Royal Society of Chemistry 2019.

involves the pouring of polymer solution into a casting mold containing the 3D scaffold. Typically, the 3D scaffold is cut into pieces, and then a thick layer of polymer solution is dispensed into the bottom of the mold. The scaffold pieces are then placed over the polymer solution. Another layer of polymer solution is uniformly dispensed over the scaffold, and the assembly is left to cure at a specified temperature. This approach facilitates the complete impregnation of the 3D scaffold with the polymer solution. The polymer impregnates through the pore and coats the branches of the scaffold. Fig. 4c depicts the fabrication of the GNPs/rGO foam/epoxy composites by template method, where the prepared GNFs/rGO scaffold acts as a template over which the liquid polymer is filled.

It is notable that only certain polymers (such as PDMS, epoxy) have been used to formulate a composite with the 3D graphene scaffold. This is likely due to the low viscosity of a polymer like PDMS, which facilitates its easy infiltration into the 3D scaffold. Also, the ease of processing and availability of those polymers with different viscosities provides the freedom to choose different fabrication techniques, such as coating, vacuum infiltration, 3D printing, *etc*. On account of their structural capabilities and good adhesion properties, epoxy and PDMS have been preferred polymers, which can be either coated or impregnated to develop 3D graphene scaffold composites. Furthermore, the presence of excellent surface chemistry between those polymers and the graphene scaffold enables the excellent wettability of the polymer onto the 3D structure.[34] The low viscosity and improved wettability facilitate robust interfacial interactions between the polymer and 3D scaffold, which promotes the formation of a network, thereby increasing the electrical conductivity.

5. 3D graphene aerogel/foam-based polymer composites for EMI shielding

Graphene aerogels and foams represent a novel class of highly interconnected 3D cellular structures with a unique blend of physical properties. They are lightweight yet offer desirable electrical conductivity, providing multiple reflection loss and internal scattering sites. The porous structure with air pockets not only confronts permeating radiations through multiple reflections and scattering within the cells, but also improves impedance matching, thereby minimizing the secondary reflection and enhancing the overall EM wave attenuation ability *via* polarization relaxation loss. In graphene-based aerogels and foams, dielectric loss plays a key role in EMI attenuation, which is governed by electrical conductivity, polarization relaxation and multiple scattering.[69] Optimum tailoring of the electrical conductivity and dielectric properties is required to realize a high-performance EMI shielding material,[27] as

Schelkunoff's transmission theory suggests that the electrical conductivity of the shielding material should be modulated and kept moderately high. GAs and foams form intricate conductive networks that enlarge the electron conduction path and dissipate the EM radiation. The so-formed conductive scaffold induces a current in the EM field, thereby absorbing the EM waves and converting them into thermal energy. In addition, it can be exploited as a framework onto which other magnetic or dielectric loss particles can be incorporated to further improve the shielding performance *via* conduction and polarization losses. The adjusted conductivity of GAs and foams, along with the additional edge atom defection, contribute to the conduction and polarisation relaxation loss. It is interesting to note that the macro-properties of GAs (radiation absorption) can be tailored by varying the pore size, resulting in a wide bandwidth absorption. Graphene aerogel–epoxy composites (GA–EP) were prepared by an infiltration technique using a porous GA scaffold.[51] The sizes of GO were varied to tune the cellular structure of GA with different pore sizes and morphologies, and the pore size-dependent shielding performances were studied. Interestingly, the GA obtained from large-sized GO (LGA) after compounding with epoxy exhibited superior shielding and mechanical properties compared to that of the composites achieved from small-sized GA graphene (SGA). The LGA–EP composites with 1.0 wt% filler and at a thickness of 3 mm showed an EMI shielding effectiveness (EMI SE) value of ~30 dB and compressive strength of 56.01 ± 1.57 MPa. The significant improvement in EMI SE at such a small loading of filler was ascribed to the unique interconnected network structure formed by the large-sized GO, which provided a wide channel for fast movement of the charge carrier. Furthermore, the generation of numerous solid/air interfaces tuned the surface impedance matching and prolonged the EM wave transmission path inside the composites *via* internal scattering. It is interesting to observe that by controlling the sizes of the precursor of the 3D scaffold, the electrical properties and impedance (and hence, the structure-EMI shield performance) can be tailored. Fig. 5(a–d) shows the microstructures of LGA and SGA, which clearly depict the formation of different pore size morphologies emerging from different size precursor GO nanoparticles.

In general, a high weight percentage of conductive fillers is required to construct a seamless electric network for composites with randomly oriented porous scaffolds. Therefore, to

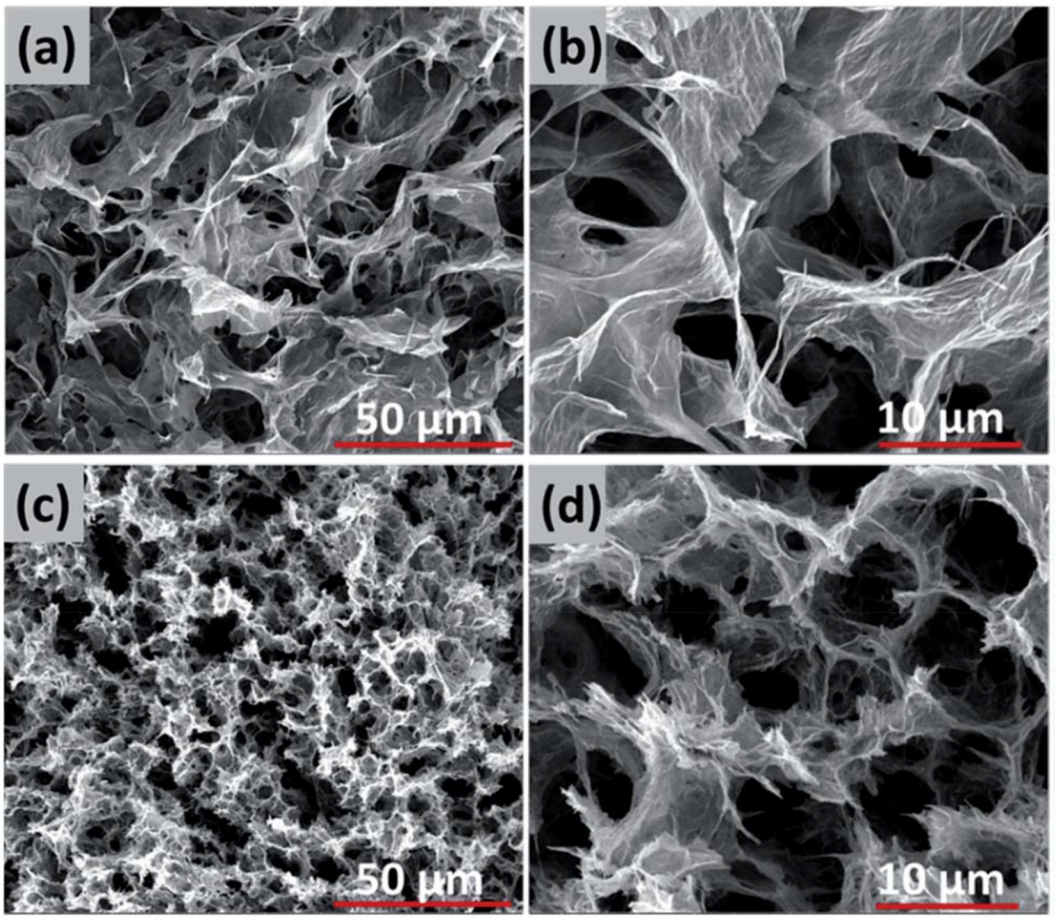

Fig. 5 Scanning electron microscopy micrographs showing the different microstructures. (a & b) Aerogels achieved from large size GO, and (c & d) obtained from small size GO; reproduced with permission from ref. 51, copyright reserved Royal Society of Chemistry 2016.

further lower the percolation threshold in porous structures, different strategies have been pursued to fabricate 3D conductive scaffolds with oriented structures.[37] A 3D architecture with a highly oriented structure shows higher electrical conductivity at low filler content, thereby achieving high-performance shielding efficiency. To exploit the orientation-dependent EMI shielding properties, GAs with anisotropic microstructures have been used to fabricate composites for EMI shielding.[70] Anisotropic GAs (AGAs) with highly aligned graphene networks were prepared by self-assembly of rGO, followed by directional freeze-drying method. Remarkably, the prepared AGAs scaffold showed different microstructures and performances along the axial (freezing direction) and radial (perpendicular to the axial direction) directions. Epoxy resin was impregnated within the AGAs scaffold assisted by vacuum. The highly aligned graphene/epoxy composite showed an EMI shielding effectiveness of 32 dB along the radial direction with 0.8 wt% thermally treated AGAs (TAGAs) coupled with the improved storage modulus. The shielding contribution from SE_A along the radial direction was found to be higher than those along the axial direction. This is likely due to the hierarchical alignment of graphene sheets that increase the propagation path length of the EM wave. Due to the presence of numerous multifaceted surface areas rendered by GAs, the permeated wave suffers multiple reflection and scattering, resulting in the decay of radiation. The result reveals that confining the graphene nanosheets in the preferred direction could be more effective in designing a shielding material with absorption-dominated characteristics. A nacre-mimetic graphene network prepared by a unique bidirectional freezing technique incorporating polymer composites (with 0.42 wt% graphene) has revealed an EMI SE (~65 dB) that is comparable to that of copper foil.[37] The bidirectional freezing technique was adopted over unidirectional freezing to create a long-range aligned lamellar structure with tunable interlayer spacing and layer thickness. The prepared composites displayed anisotropic conductivities and mechanical properties, along with significant shielding performance, which was found to be dependent on the architecture of the 3D conductive network. The biaxially aligned lamellar structure creates many efficient interfaces within the composites, promoting multiple interlayer reflections that consume the electromagnetic radiation. The impact of the architecture of the conductive channel on SE, such as high layer density (more lamellar interfaces), was found to contribute more to absorption. The realization of such a high value of EMI SE at low filler loading indicates that to harness the optimum loss ability of the conductive filler, the meticulous design of a 3D scaffold is crucial for the development of high-performance EMI shielding polymer composites. Song *et al.* prepared rGO with a honeycomb structure (rGH) following freeze-drying & thermal annealing using an aluminium oxide (Al_2O_3) honeycomb as a template, which was then immersed into epoxy resins to fabricate rGH/epoxy composites that showed an EMI SE value of 38 dB.[71] The improvement in SE was attributed to the multiple reflections within the honeycomb pores, and to the attenuation of the EM waves as it induces current inside rGH.

Chen *et al*. prepared porous GAs enhanced with phenolic resol resin by hydrothermal procedure, followed by annealing and incorporation into the epoxy resin to study the EMI shielding performance.[72] It was believed that phenolic resol resin assisted the graphene sheets in coalescing into a hierarchical 3D macrostructure, assumed to be preserved during compounding with epoxy resin. The prepared AG induced high electrical conductivity within the epoxy resin, and the composites showed excellent EMI shielding performance. With the addition of only 0.33 wt% of the annealed aerogel, an electrical conductivity value of 73 S m^{-1} and an EMI shielding effectiveness value of 35 dB were recorded. The report systematically investigated the effects of thickness on the shielding performance, and it was found that as the sample thickness increased, the EMI shielding performance also increased. In another study, graphene-based aerogel film (AF)/PDMS composites have been prepared to explore the EMI SE of AF in a polymer matrix.[73] The following infiltrating and curing single and multilayer rGO-AF/PDMS composites were prepared. The five-layer rGO-AF/PDMS composite with a density of 0.122 g cm^{-3} and a thickness of 1.547 mm exhibited an SE value of 53 dB at the X-band (8.2–12.4 GHz), and a specific SE of up to 434 dB cm^3 g^{-1}. The single-layer composite exhibited a reflection-dominated mechanism at lower frequencies, while absorption dominated at higher frequencies. Increasing the number of composite layers does not significantly impact the reflection efficiency. However, the absorption efficiency shows an increasing trend. The model presented earlier in this review article can be employed to understand how changing the thickness of the layer influences the EM absorption ability. The amount of secondary reflection can be minimized by adjusting the layer thickness of the material. Achieving strong loss ability and better impedance matching is crucial to realizing an absorption-dominated shielding mechanism. Heterogeneous interfaces originating from more than one component can elevate the loss abilities through synergistic effects, enhancing impedance matching and interfacial polarization loss, which are vital to achieving an absorption-dominated EMI shielding mechanism. Towards this, ternary mixtures of thermally annealed GA (TAGA), MWCNT and PANI have been designed to render epoxy composites with a synergistically robust triple conductive network.[74] The PANI/MWCNT/TAGA/epoxy nanocomposites exhibited an EMI SE value of 42 dB and electrical conductivity of 52.1 S cm^{-1} at the mass ratio of 3 : 1 (GO to f-MWCNT) and the loading of 4.61 wt%. The promising results obtained from this study suggest that modulated and customized heterogenous interfaces can be generated by composition optimization, which would enhance the electromagnetic attenuation in the 3D graphene-based hybrid. There has been an upsurge in research activities on multifunctional composites, as current technologies expect a material to have more than one property and perform more than one function. A single attribute of a material is not enough if it is to be applied in a complex environment. Taking that into consideration, recent research studies are focused on designing composites with dual func-

tionality or more. Recently, a 3D copper nanowires-thermally annealed graphene aerogel (CuNWs-TAGA) framework that was prepared by freeze-drying, followed by thermal annealing, was reported.[75] Epoxy resin was poured into the prepared framework to achieve CuNWs-TAGA/epoxy composites for high thermal conductivity and EMI shielding effectiveness. It is worth noting that the composites revealed a thermal conductivity coefficient (λ) value of 0.51 W m^{-1} K^{-1}, EMI SE value of 47 dB, and electrical conductivity (σ) of 120.8 S m^{-1}. It is likely that the compounding of CuNWs and GA resulted in an abundant heterogeneous interface that was conducive to enhancing loss efficiency. It can be concluded that if the selection of the material is made prudently, it is possible to induce abundant heterogeneous interfaces, thereby enhancing the EM wave attenuation.

The colossal, interconnected network formed by the nodes and branches of graphene foam within the polymer matrix creates seamless channels for the rapid transfer of electrons. However, care must be taken to develop high-quality GF as the inter-sheet junction contact resistance lowers the electrical conductivity of GF. In an endeavour to improve the quality of the foam or decrease the inter-sheet junction contact resistance, the template-directed CVD method has been reported to design graphene/poly(dimethyl siloxane) (PDMS) foam composites.[6] The amount of graphene and the electrical conductivity of the composites were tuned by varying the flow rate of methane during the CVD growth of graphene. The prepared composites exhibited a density of ~0.06 g cm^3, which is 20 times less than that of a solid polymer composite. With the loading of <0.8 wt%, an EMI SE as high as 30 dB was recorded with a specific EMI SE of up to 500 dB cm^3g^{-1}. Furthermore, the foam composites showed excellent flexibility, and their SE remained unaltered after repeatedly bending to a radius of ~2.5 mm for 10 000 times. The demand for lightweight electrical components crucial in applications such as next-generation aircraft and wearable devices has elevated the relevance of flexible polymer composites more than ever before. In this regard, continuous attempts have been made to develop flexible composites with superior EMI shielding efficiency, along with other attributes such as lower density and flexibility. Towards this, PDMS was directly infiltrated into a 3D interconnected graphene network using the vacuum-assisted technique.[76]

The super flexible composites showed an excellent electrical conductivity value of 103 S m^{-1} and EMI SE of around 54 dB with 3.07 wt% of graphene. A majority of the EM wave was absorbed by the composite, which made a significant contribution to the overall shielding mechanism. It was assumed that the 3D interconnected scaffold formed numerous multifaceted cells, promoting multiple reflections, and scattering that made the escape of the microwaves difficult. The presence of residual polar functional groups, defects, and multiple interfaces contributes to dipole polarization loss, thereby contributing to the overall loss mechanism. The development of a highly porous, bendable laterally compressed GF (cGF)/acrylonitrile butadiene styrene (ABS) composite with seminal shielding and certain strength has been reported to confer structural stability and superior shielding.[32] The composite was prepared by dip coating ABS on a dense cellular anatomy of freestanding cGFs, which was achieved by growing graphene on laterally compressed Ni foam substrates. Isotropic cellular graphene foams were achieved, with similar openings between the skeletons along both the compression direction and perpendicular to it. The cellular foam retained its structure even after ABS was drop coated. It is worth noting that the composites showed a porosity of 89% and ultra-low density of 0.12 g cm^{-3}. The 75%-cGF/ABS composites exhibited a distinctive two-layer structure comprising the cellular porous structure with ABS evenly coated on the graphene networks. The cGF/ABS system with a graphene content of 8 wt% delivered an electrical conductivity value of 635 S cm^{-1} and SE of 42.4 dB (at 50% compression), along with robust and bendable performances. These cGF/ABS composites display superior mechanical properties over other flexible polymer systems, such as GF/PDMS composites of comparable density.[76] The absorption-dominant EMI shielding was ascribed to the efficient dissipation of surface currents by the high-quality meticulously designed graphene skeleton and quick thermal losses. Moreover, the laterally compressed GFs rendered denser graphene structures, leading to denser conductive networks per unit volume. The shielding performance of the composites decreases with the further rise in lateral compression degree (above 50%), which is indicative of annihilation of the conductive network at a higher degree of compression. This study reveals interesting findings that the electromagnetic absorption performance of the composites can be modulated by regulating the compression strain during scaffold growth. Ba *et al.* created a 3D network of graphene (TPU/G) by employing sodium chloride (NaCl) as the template and thermoplastic polyurethane (TPU) as the binder, which was subsequently carbonized to generate the C/G network, and encapsulated in epoxy resin.[77] At 1.59 wt% of graphene loading, the SE value reached ~38.78 dB. Meanwhile, at 7.60 wt% of graphene, the thermal conductivity value reached 1.19 W m^{-1} K^{-1}. It is interesting to note that with the increase in the graphene content, the absorption coefficient values diminished, which is likely due to enhanced reflection with the accumulation of graphene sheets. In another report, microporous ultrathin graphene nanosheet foams have been reported by a salt-template-driven freeze-drying-calcination route with PEG 20 000 and NaCl as a carbon source and a template, respectively.[78] The calcination temperature (T) and PEG 20 000/NaCl mass ratio (λ) were unutilized to modulate the texture, defects, graphitization, EMI SE, and thermal conductivity of the graphene foams. The graphene foams were created under T = 800 °C and λ = 0.530, and subsequently compounded with silicone rubber, exhibiting the optimal EMI SE and thermal conductivity, *viz.*, 3.95 W $(m\ K)^{-1}$ and EMI SE > 20 dB, respectively. The enhancement in SE was ascribed to the conductive loss (ε''_c), polarization loss (ε''_p), and multiple scattering that arose due to the strong shape anisotropy of the ultrathin graphene nanosheet foams, large

specific surface area, high defects, small thickness, and porous 3D crosslinked frameworks. Conducting 3D networks at lower mass concentration of filler have been prepared by modifying GF using *p*-phenylenediamine (PPD), which anchors the reactive sites on GF for further *in situ* polymerization of PANI, leading to the formation of the network structure of GF/PANI.[79] It is speculated that PANI promoted the connection of graphene sheets in GF, enabling the formation of the connecting network. After being compounded with epoxy, GF/PANI exhibited an EMI SE value of 38.32 dB. A novel leaf-like structure foam composed of CNTs and rGO (abbreviated as CGF) had been reported to reduce the density of the 3D structure, which was subsequently compounded with PDMS for EMI shielding applications.[35] The presence of CNTs enabled the expansion of the conductive network and increased the electrical conductivity by 274.4%. The CNTs were firmly embedded into the graphene hole *via* π–π interactions. The leaf-like structure foam material exhibited a SE value of 71.4 dB. When compounded with PDMS, the composites retained 71.6% (71.1 dB to 50.9 dB) of SE after pressing 100 times under a pressure of 500 kPa. In another study from the same research group, a leaf-like 3D CNTs/GA film (CGAF) was designed, where CNTs were impeccably embedded in graphene, akin to the veins and mesophyll of a leaf.[38] The prepared 3D CGAF scaffold exhibited an EMI SE value of 26.6 dB, which predominantly arose from the absorption of the EM wave rather than reflection. On compounding the CGAF scaffold with PDMS, an EMI SE value of 74.7 dB was reported, which corroborated the efficient flow of charges in the conducting network formed by seamlessly embedded CNTs and consumption of EM waves due to the multiple reflections in the 3D structure.

Drop coating of poly(3,4-ethylenedioxythiophene):poly (styrene sulfonate) (PEDOT:PSS) on 3D freestanding GFs has been performed to fabricate GF/PEDOT:PSS composites for EMI shielding applications.[80] The GF/PEDOT:PSS composites exhibited an ultralow density of 18.2×10^{-3} g cm^{-3} and a porosity of 98.8%, as well as an electrical conductivity value of 4320 S m^{-1}. The so-formed highly conducting network and porous macro-structure assisted in the smooth transport of electric charge, which resulted in an SE value of 91.9 dB. The increased dielectric loss promoted the decay of the penetrating radiation, which led to a high absorption of EM waves. Dielectric loss of the composite is basically ruled by three electronic processes, *viz.*, electronic displacement, space charge and interfacial polarization.[81,82] It is likely that the network channel generated by the 3D macrostructure rendered a pathway for electromagnetic field-induced currents, resulting in the rapid decay of radiation. Fig. 6a shows the preparation of the free-standing graphene scaffold and composites, and the morphologies of the foam before and after coating (Fig. 6c and d), where a uniform coating of PEDOT:PSS can be seen on the 4-dodecylbenzene acid (DBSA)-functionalized graphene foam (Fig. 6d). The decrease in contact angle (Fig. 6e) with the increase in the concentration of DBSA indicates enhanced interactions of PEDOT:PSS with the graphene foam (Table 1).

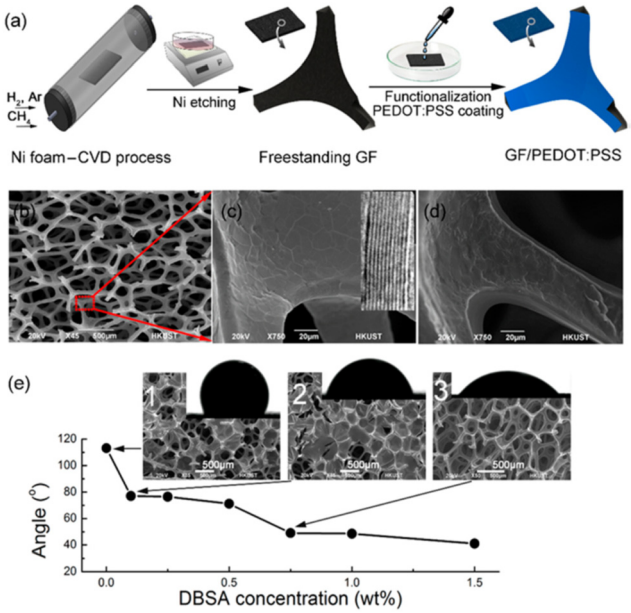

Fig. 6 (a) Schematic procedure of the preparation of the GF/PEDOT:PSS composites; (b and c) SEM and TEM images of GFs before and (d) after PEDOT:PSS coating and (e) contact angles of the compressed GF plates as a function of the DBSA concentration. The inset in (c) is the TEM image of pristine graphene. The insets in (e) show the SEM images of the GF/PEDOT:PSS composites treated with different DBSA concentrations and the shapes of the corresponding PEDOT:PSS droplets (1, no treatment; 2, treated with 0.1 wt% DBSA; and 3, treated with 0.75 wt% DBSA), reproduced with permission from ref. 80, copyright reserved American Chemical Society 2017.

6. 3D graphene/2D, 1D heterostructure-based polymer composites for shielding material

Recently, the fabrication of graphene-based 3D structures with synergistic conductive networks has garnered wide attention. Although hierarchical polymer composites exhibit significant improvements in electrical conductivity compared to directly introduced filler composites, there still exists a prospect to further enhance the performance by tailoring the reduced graphene oxide (rGO)-based 3D (dispersion and dielectric properties) structure through the embedding of additional particles (2D, 1D, 0D particles). Secondary conductive fillers (such as graphene nanoplatelets (GNPs), CNTs, *etc.*) have been used along with the 3D rGO to generate a synergistic giant conducting scaffold for the efficient transport of charge carriers, and as dielectric loss components to enhance the absorption mechanism. CNTs significantly enhance the polarisation relaxation, conduction, and dielectric loss. GNPs have been embedded in the 3D rGO foam to fabricate 3D porous GNPs/rGO foam/epoxy (GNPs/rGO/EP) nanocomposites *via* template method.[83] Embedded GNPs improve the electrical conductivity and assist in the formation of a seamless conducting channel for the fast and efficient transport of charge carriers. The

Table 1 Examples of graphene aerogel/foam-based polymer composites with their EMI SE attributes

Materials	Loading %	Preparation method	σ, S m^{-1}	EMI SE (dB)	Ref.
GA/epoxy	1.0	Infiltration technique	—	30	51
Anisotropic GA/epoxy	0.8	Vacuum infiltration	—	32	70
GA/phenolic resin	0.33	Vacuum infiltration	73	35	72
Aerogel film/PDMS		Vacuum infiltration		53	73
GA/PDMS	0.42	Self-assembly	0.5	65	37
GA/MWCNT/PANI/epoxy	4.61	Template-casting method	52.1	42	74
CuNW/GA/epoxy	—	Back filling	120.8	47	75
rGO honeycomb/epoxy	1.2	Back filling	40.2	38	71
GF/PDMS	0.8	Dip coating		30	6
GF/PDMS	3.07	Vacuum infiltration	103	54	76
GF/ABS rubber	8	Dip coating	635	42.4	32
Porous graphene/epoxy	1.59	Vacuum infiltration	318.48	38.78	77
GF/Silicon rubber	7	—	51.84	>20	78
GF/PANI/epoxy	—	Dip coating	—	38.32	79
CNTs/rGO foam/PDMS	—	Simple immersion	—	71.1	35
GNPs/rGO foam/epoxy	rGO : GNPs 0.1 : 20.4	Template method	179.2	51	83
CNT/graphene aerogel/PDMS	—	Simple immersion	—	74.7	38
GF/PEDOT:PSS	—	Drop coating	4320	91.9	80

GNPs/rGO/EP nanocomposites containing 0.1 wt% rGO and 20.4 wt% GNPs reveal an EMI SE value of 51 dB, an almost 292% improvement as compared to the rGO/EP nanocomposites (~13 dB) and 240% enhancement relative to the GNPs/EP nanocomposites (~15 dB). Furthermore, the nanocomposites exhibited an excellent thermal conductivity of 1.56 W m^{-1} K^{-1} and electrical conductivity of 179.2 S m^{-1}. With the increase in the GNP content, the shielding mechanism becomes absorption-dominant, which is ascribed to the dissipation of electromagnetic waves due to improved conduction and dielectric loss. The construction of a scaffold to improve the continuity of the conducting 3D framework is a potential route to enhance the shielding performance of composites. A unique 3D hybridized carbon nanostructure was prepared by *in situ* growth of vertical edge-rich graphene (ERG) on the rGO aerogel skeleton, which was then applied to modify epoxy resin for EMI shielding and thermal management.[84] The developed rGO-ERG/epoxy nanocomposites exhibited an enhanced EMI shielding performance of 45.9 dB in the X-band, which was ascribed to the structural defects and strong charge polarization ability of ERG. In addition, theoretical models confirmed the construction of phonon-matching 3D rGO-ERG networks that resulted in efficient phonon transport, leading to a thermal conductivity value of 1.96 W m^{-1} K^{-1}. The study revealed that covalent bond connections in 3D structures not only reduce thermal resistance and phonon scatterings, but also provide a continuous conductive channel for smooth charge transport.

A facile bubble-template based strategy has been employed to create a 3D graphene network, wherein GO was employed to assist the assembly of GNP into a 3D porous framework structure.[85] Vacuum-assisted infiltration of the liquid PDMS onto the as-prepared 3D skeleton was followed to fabricate the composites, which revealed a remarkable EMI SE of around 90 dB and a high thermal conductivity of above 3 W (m K)$^{-1}$ with only 18.1 wt% of graphene content. Fig. 7a shows the optical microscope image of the foaming dispersion, wherein bubbles are seen to be uniformly distributed and closely packed together. Fig. 7b & c displays the digital images of the dried 3D rGO-GNP foam, which was able to endure a load that far heavier than its own. Fig. 7d–f depicts the microstructure of the as-developed 3D rGO-GNP foams with varying graphene contents. As discernible from the micrograph, the spherical holes left by the air bubbles are uniformly located in the foam scaffold. After careful observation, it is evident that as the graphene content increases, the extent of closure of each pore also increases. The 3D rGO-GNP-PDMS composites exhibited different contributions to the overall shielding with and without the annealing of 3D rGO-GNP. When using 3D rGO-GNP without annealing, both absorption and reflection contribute to the shielding, while annealing 3D rGO-GNP results in a more prominent contribution from reflection. It is assumed that annealing increases the electrical conductivity of 3D rGO-GNP by repairing damages on the graphene surface, rendering it a defect-free seamless conducting channel, which leads to the reflection of the EM wave. The 3D structures of the graphene nanoplatelets (GnP) and graphene fluoride (GF) have been fabricated in PDMS composites to study their EMI SE and thermal conductivity properties.[86] The porous GnP@PDMS/GF composites showed an EMI SE value of 50.13 dB against 51.26 dB for only GnP@PDMS, which was attributed to the high conductivity of GnP and porous interconnected network responsible for the attenuation of the EM waves.

In another study, a synergistic interconnected conductive network was generated by using pristine SWCNTs as secondary conductive fillers to prepare the rGO/SWCNTs aerogel.[87] The PDMS/rGO/SWCNTs nanocomposite was developed by a facile backfilling approach to explore the EMI shielding properties. The compatibility of GO enabled SWCNTs to disperse uniformly within the polymer matrix, preserving the high conductivity of SWCNTs in the developed scaffold. The composites showed an electrical conductivity value of 120 S m^{-1} and an EMI SE of ~31 dB over the X-band frequency range with an ultralow loading of 0.28 wt%. The unrivalled properties

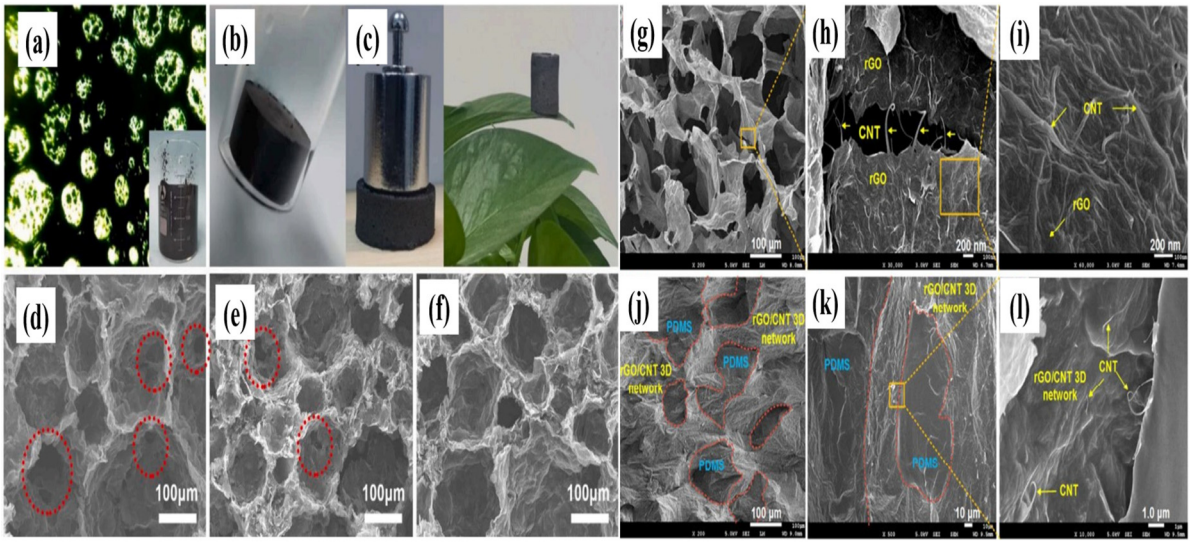

Fig. 7 (a) Optical microscopy image of the foaming emulsion, photographs of (b) the hydrogel and (c) the dried 3D rGO-GNP foam. Fracture surface SEM images of the 3D rGO-GNP foam with (d) 9.7 wt%, (e) 14.0 wt%, and (f) 18.1 wt% graphene content; reproduced with permission from ref. 85, copyright reserved Elsevier 2021. (g–i) Micrographs of the highly porous 3D TGCA3 aerogel and the fracture surface of the corresponding PTGCA3 composite (j–l) at different magnifications, where the SWCNTs nanostructures are firmly entangled with graphene; reproduced with permission from ref. 87, copyright reserved American Chemical Society 2018.

improvement ascertained the excellent synergy between rGO and SWCNTs in the aerogel system, contributing to significant dielectric loss. Fig. 7(j-l) shows the SEM images of the highly porous and interconnected 3D scaffold, where the entangled SWCNTs are wrapped into graphene sheets or act as efficient bridging to connect adjacent graphene layers. In another endeavour of a synergistic conductive network strategy, a highly porous GFs/CNTs/PDMS composite was fabricated.[88] GFs were synthesized on a Ni substrate by CVD approach, and were mixed with the CNTs/PDMS suspension to fabricate the composites. The incorporation of CNTs in PDMS was found to significantly influence the charge transport property in the GAs/CNTs hybrid. The unique 3D hybrid composites with a porosity of 90.8% exhibited an EMI SE of 75 dB, an enhancement of 200% against 25 dB of the GFs/PDMS composites with the same graphene content and porosity. The significant improvement in the SE of the hybrid composites was attributed to the synergistic effect of GA and CNTs. While graphene aerogels absorb the EM wave by dissipating currents induced by electromagnetic fields, carbon nanotubes enhance the surface current dissipation by providing interconnected conductive networks and numerous interfaces for multiple reflections and polarization loss. The contribution of SE_A towards the total SE was more prominent than that from SE_R, which is likely due to the extensive dissipation of surface currents. Employing the simple filtration and calcinations method, a 3D interconnected network was prepared using thermally treated graphene (G) and reduced oxidized multi-wall carbon nanotubes (r-OCNTs).[89] A highly conducting flexible PDMS composite cake (TCGPC) was fabricated by coating PDMS onto the thermally treated r-OCNTs/G composite. The composite cake showed an electrical conductivity value of 15.15 S cm^{-1}, which was attributed to the synergistic contribution of G and r-OCNTs. The EMI SE value was found to increase from ~50.3 dB for G/PDMS to ~67.3 dB for the composite cake in the X-band. It is important to note that the composite cake exhibited a stable EMI SE value with only 6.8% decrease after bending for 10 000 times, which suggested that it was still able to block 99.99995% of the radiation. The remarkable improvement in the average SE was ascribed to the synergy in the conductive network provided by CNTs, as well as the enhanced electrical conductivity induced by calcinations. The composite cakes showed an absorption-dominated mechanism, which indicated that most of the EM decays into thermal energy *via* dielectric loss and interfacial polarisation loss. The energy consumption activity is accounted to the relaxation loss through interfacial polarisation and surface charge. Using the 3D graphene/MWCNTs foam as an electrically conductive skeleton, PDMS composites were fabricated for EMI shielding applications.[90] The structure and composition evolution of the prepared foams were studied during the carbonization process from 1200 to 1600 °C and the graphitization at ultra-high temperature (2800 °C). It is considered that with the annihilation of polar functional groups, the repair of defects augments the ohmic loss while the polarization loss is reduced. An SE value of 54.43 dB at 1400 °C was reported. MWCNTs basically performed the three functions. First, it acts as a bridge to connect the gap between the 2D graphene sheets, rendering efficient electronic channels to the structure. Second, it functions as an impediment to the agglomeration of graphene sheets. Lastly, some MWCNTs extend to the outer edge of the graphene sheets, and act as electron polarization centres. The likely mechanism for such an improvement in SE was attributed to ohmic loss and polarization loss (electronic,

dipole polarization), which is depicted in the interaction model diagram (Fig. 8a and b). Through this loss mechanism, the EM wave is mostly converted into heat and dissipated. In this study, the heat dissipation (measured as increased in temperature) was studied using infrared thermography, which is depicted in Fig. 8d. As indicated by the higher temperature, the thermal transfer rate in the composites seems superior to that of neat PDMS. As depicted in Fig. 8c, the developed composites show enhanced compressive strength, and the strength increases with the annealing temperature.

The design of a secondary conductive network conducive for EMI shielding using 3D graphene has emerged to assist in the dispersion of the conductive filler.[91] A 3D silver platelets/rGO foam (AgPs/rGF) with numerous regular spherical hollow structures has been reported, wherein AgPs are uniformly dispersed along the rGO network assisted by 3D graphene.[92] The interconnected 3D rGO channel resolved the agglomeration propensity of AgPs, and was eventually assembled with the secondary conductive network. Epoxy nanocomposites were prepared by backfilling the epoxy system on the 3D AgPs/rGF scaffold, which exhibited an electrical conductivity value of 45.3 S m^{-1} and SE 58 dB in the X-band with 0.44 vol% rGF and 0.94 vol% AgPs. The incorporation of AgPs shifted the shielding mechanism from an equal contribution of reflection and adsorption to being reflection-dominant. The study also validates the shielding ability of the 3D AgPs/rGF/EP nanocomposites to defy EM radiation by employing a finite element model to simulate the radiation process of the EM waves generated by the communication antenna to the brain, which is depicted in Fig. 9. A 12 V antenna was used for radiating EM waves to exposed and protected brain (protected by 3D AgPs/rGF/EP nanocomposites). Fig. 9d–d″ depicts the map of the electric field distribution in the brain protected by 3D AgPs/rGF/EP, where the intensity of the radiated electric field is considerably reduced in air and the brain is seen to be almost unaffected. A study on Ag nanoparticle-decorated 3D porous rGO/polybenzoxazine composites also revealed enhancement in SE due to multi-reflections and current-induced magnetic dipoles.[93] The magnetic losses-enhanced absorption mechanism led to an EMI SE value of 54 dB for the mentioned composites.

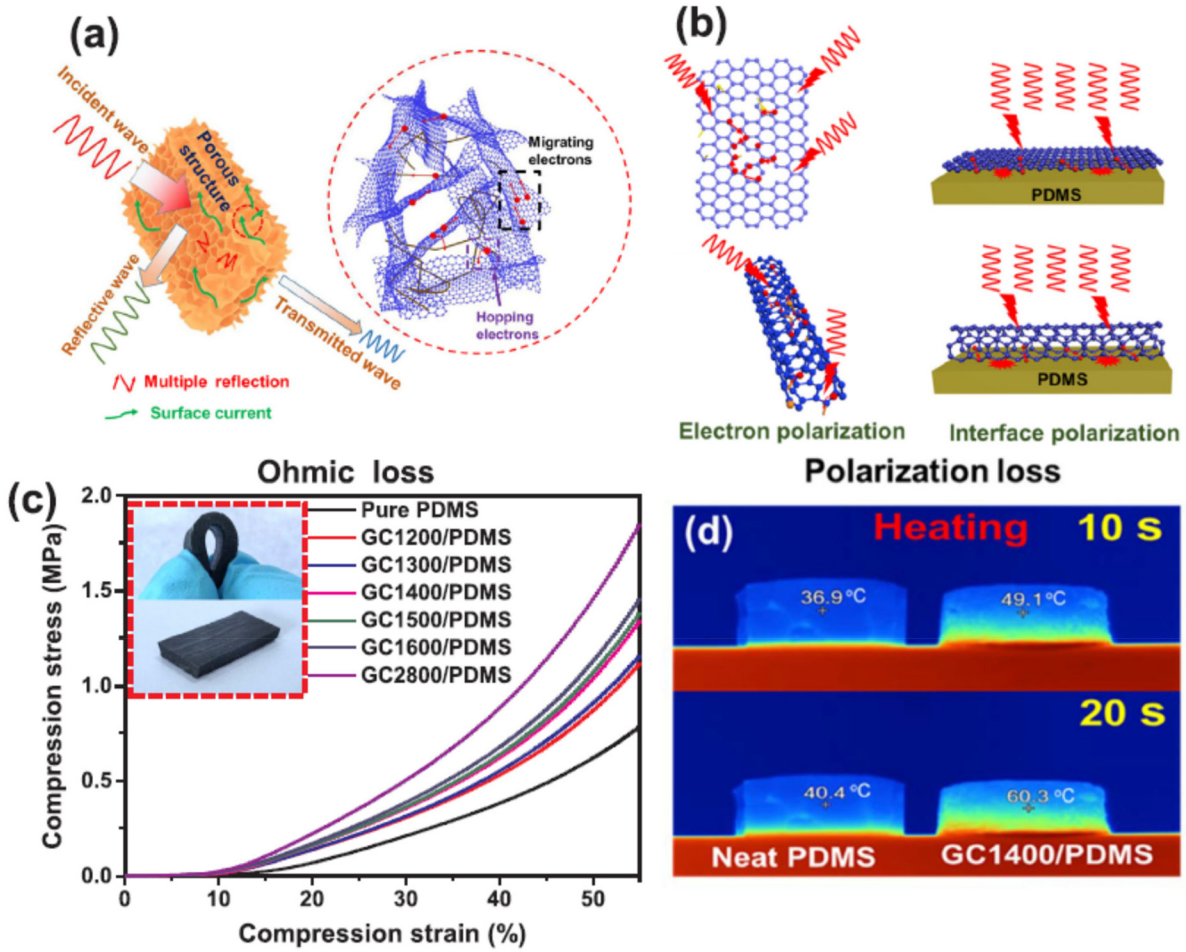

Fig. 8 (a and b) Schematic diagram of the EM shielding mechanism of the GC/PDMS composites. (c) Compression stress–strain curves of GC1400/PDMS and neat PDMS. The inset shows the optical images of GC1400/PDMS and the bent GC1400/PDMS. (d) Infrared thermography images of GC1400/PDMS and neat PDMS in heating for 10 s and 20 s (the hot stage with a temperature of 150 °C); reproduced with permission from ref. 90, copyright reserved Elsevier 2020.

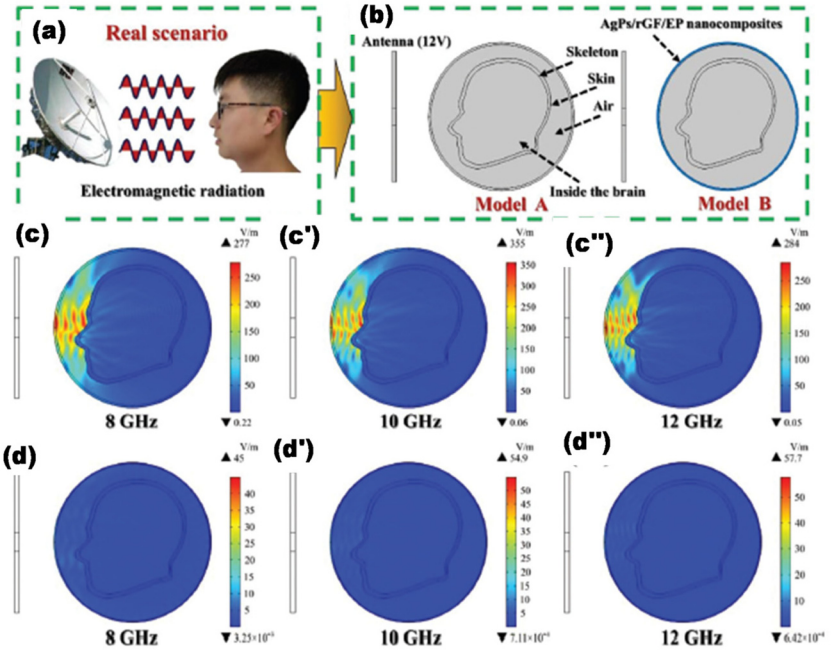

Fig. 9 Brain simulation exposed to electromagnetic radiation from the communication antenna. (a) Schematic diagram of the model prototype; (b) simplified radiation model. Model A: directly exposed brain to the electromagnetic radiation. Model B: protected brain to the electromagnetic radiation by 3D AgPs/rGF/EP nanocomposites; (c–c″) map of the electric field distribution in the brain; (d–d″) map of the electric field distribution in the brain under the protection of the 3D AgPs/rGF/EP nanocomposites. Reproduced with permission from ref. 92, copyright reserved Royal Society of Chemistry 2019.

Aqueous GOs dispersants and one-dimensional (1D) silver nanowires (AgNWs) have been chosen to construct 3D rGOs/AgNWs bi-continuous conductive skeletons (GACSs).[94] To minimize the high inter-sheet contact resistance and impede the agglomeration of rGO nanosheets, AgNWs were selected as a secondary building block to construct a 3D conductive scaffold. A modified sol–gel technique was applied to develop the GOs/AgNWs scaffold, which increased the pore sizes, pore-wall thickness, and structural homogeneity of the resulting composite scaffold. The scaffold was used to fabricate polydimethylsiloxane composites (PGACs) and the electrical, EMI shielding, and other properties were investigated. A series of PGACs were prepared, keeping constant the rGOs loading of 0.43% and varying the AgNWs loading, and they are represented as PG5A1C-0.53%, PG3A1C-0.6%, PG2A1C-0.66%, and PG3A2C-0.76%, respectively. The EMI SE of PGACs in the X-band was found to increase with the increase of the AgNWs amount, and reached the highest EMI SE of 34.1 dB at 0.43 wt% rGOs and 0.33 wt% AgNWs loadings. A significant enhancement in EMI SE was assigned to the synergy in conductivity between rGOs and AgNWs. Fig. 10 shows the variations of electrical conductivity, SE_T and the corresponding contribution from SE_A and SE_R. According to Fig. 10b–d, the significant contribution to the total shielding was from the absorption-induced shielding. Conversely, the reflection is minimal, attributed to effective attenuation of the EM wave promoted by the 3D scaffold. With the higher electrical conductivity and improved impedance matching, the rapid localized current generations and faster thermal loss contribute to the total shielding.

Mimicking natural porous materials, a bio-inspired approach based on polydopamine interface buffer for the preparation of a carbon nanowires/graphene (CNWs/G) sponge composite has recently been reported.[95] CNWs were uniformly grown on the graphene structure through covalent C–C bonding. A multi-scale structure was designed to maximize the absorption mechanism, where porous graphene behaved as a sponge skeleton and provided high electric conductivity. The *in situ* grown CNWs served as flagella that rendered strong EM absorption competency. The junction between the CNWs with graphene and the defects present in CNWs led to strong polarization loss, and hence the attenuation of the permeating radiation. The CNWs/G/PDMS composite showed an EMI SE value of 36 dB in the X-band and the composite density was found to be 97.1 mg cm^{-3}. The improvement in SE was attributed to the unique sponge macrostructure of graphene and CNWs with the covalent junction interface, which spawned a strong polarization loss and promoted multiple reflections of EM waves. A hybrid structure of the 3D scaffold has shown great potential in EMI shielding applications. However, achieving a mechanically robust 3D scaffold with a high SE value is still a daunting challenge. Towards this, Fan *et al.* reported the fabrication of a microcellular epoxy foam containing a hybrid reduced graphene oxide (rGO)/short carbon-fiber (SCF) aerogel following the "gelation-press drying-impregnation & micro-foaming" method.[96] The air-drying method was employed to

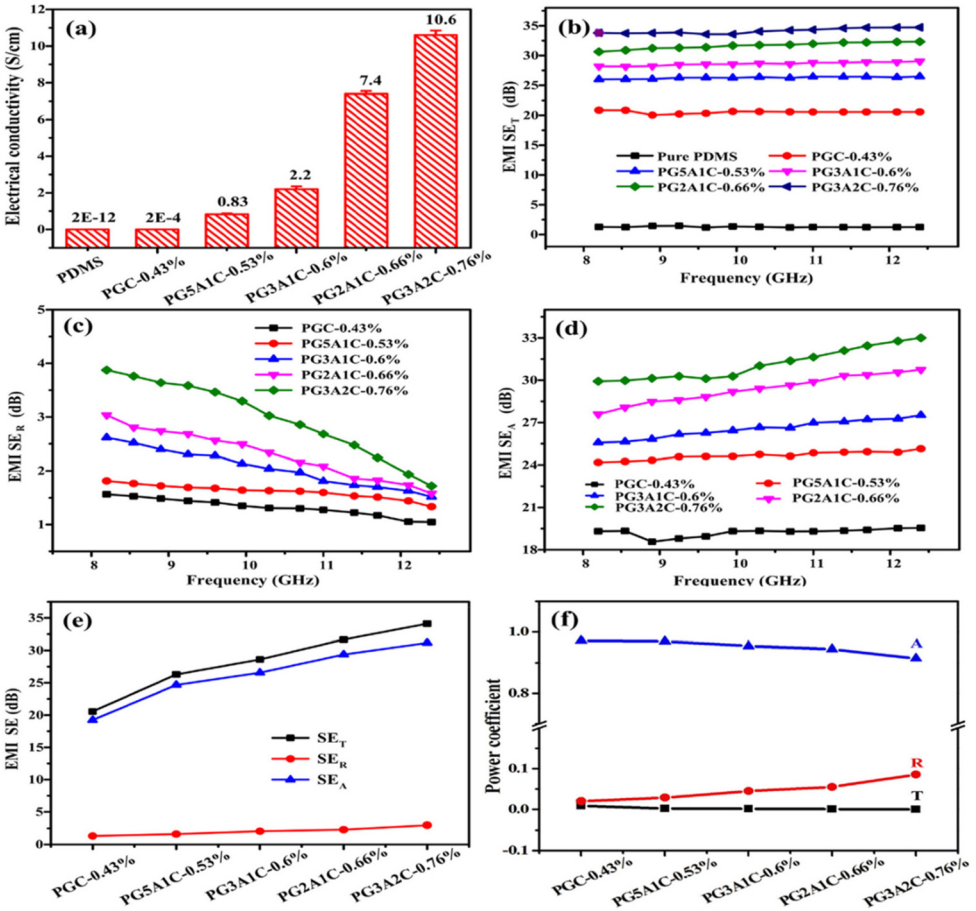

Fig. 10 (a) Electrical conductivity and (b) SE_T of PDMS, PGC-0.43% and PGACs in the X-band, (c) SE_R, (d) SE_A, (e) the average SE_T, SE_R, SE_A, and (f) the average power coefficients (A, R, T) of PGC-0.43% and PGACs in the X-band; reproduced with permission from ref. 94, copyright reserved Elsevier 2019.

control the network structure of rGO/SCF, which resulted in a transformation of the isotropic honey-comb structure into an anisotropic multilayer corrugated structure. The purpose of SCF was to provide stability to the carbon network that would keep the porous structure intact. The anisotropic microcellular epoxy composites showed an EMI shielding value of 95.5 dB (Table 2).

7. 3D graphene/magnetic heterostructure polymer composites for EMI shielding

Although the 3D graphene-based dielectric material has been successful in significantly improving the EMI SE at higher fre-

Table 2 Examples of 3D graphene/2D, 1D heterostructure based polymer composites with their EMI SE attributes

Materials	Loading %	Preparation method	σ, S m^{-1}	EMI SE (dB)	Ref.
Edge-rich graphene/rGO/epoxy	3.98	Vacuum infiltration	68.2	45.9	84
GO/GNP/PDMS	18.1	Vacuum infiltration	—	90	85
GNP/graphene fluoride/PDMS	30	Molding	0.6	50.1	86
rGO/SWCNTs/PDMS	0.28	Backfilling	120	31	87
GFs/CNTs/PDMS	GF : CNT 2.7 : 2	Simple deposition	31.5	75	88
CNTs/graphene/PDMS	—	Vacuum infiltration	15.15	67.3	89
3D graphene/MWCNTs/PDMS	0.98	Vacuum infiltration	100.99	56	90
rGOs/AgPs/PDMS	rGOs : AgPs 0.33 : 0.43	Backfilling	45.3	58	92
Ag/rGO/polybenzoxazine	Ag : rGO 15 : 25	—	0.005	54	93
rGOs/AgNWs/PDMS	0.76	Backfilling	0.108	34.1	94
CNWs/G/PDMS		Dip coating	0.34	36	95
rGO/short carbon-fiber/epoxy	—	Foaming	2365.0	95.5	96

quency, the constantly evolving next-generation technology seeks components with a broad bandwidth shielding efficiency. Pristine single-phase graphene possesses insignificant magnetic permeability and does not support the magnetic hysteresis losses mechanism. These attributes narrow down its prospect of larger range radiation absorption. Typically, an effective synergy in the magnetic loss and dielectric loss is needed to ensure high-performance shielding. According to the condition of perfect impedance matching:[97]

$$Z = \sqrt{\frac{\mu}{\varepsilon}} = 1.$$

Based on the above equation, to achieve the desirable impedance matching performance, it is crucial to make μ relatively close to ε. In order to improve loss mechanism for better EMI shielding, recently two phase heterostructures consisting of magnetic nanoparticles and graphene have evoked wide attention.[98–102] 3D graphene-based scaffolds have tunable porosity, which offers points to anchor magnetic components. Magnetic metals (such Fe, Co, Ni or their oxides) have been used with graphene or with a combination of graphene and CNTs to fabricate a 3D integrated architecture. The large single architecture, created through strong synergy, enhances EMI SE by improving the eddy current loss, natural resonance, exchange resonance, and multiple scattering processes. In addition to that, the combination of magnetic materials with the dielectric foam/aerogel improves the permeability of the scaffold, thus achieving an ideal impedance match that is conducive to the absorption-dominated shielding mechanism. The magnetic loss contributed by the magnetic medium to the overall shielding mainly arises from the exchange resonance, natural ferromagnetic resonance and eddy current loss.[103]

Towards improving the impedance matching and EM loss through magnetic materials, numerous absorption-dominated graphene aerogels or foams-based composites recently have been developed. For example, the Fe_3O_4/thermally annealed graphene aerogel (Fe_3O_4/TAGA)/epoxy nanocomposites were fabricated to study the EMI SE.[104] At first, ethylene diamine functionalized Fe_3O_4 (NH_2–Fe_3O_4) nanoparticles and GO were compounded, followed by the addition of L-ascorbic acid, to obtain Fe_3O_4/TAGA by thermal annealing method. Fe_3O_4/TAGA exhibited a pore structure, which is considered advantageous for multiple-reflection and hence for the effective attenuation of EM radiation. The Fe_3O_4/TAGA/epoxy nanocomposites showed an electrical conductivity value of 27.5 S m^{-1} when the mass ratio of GO to NH_2–Fe_3O_4 was 2 : 1 and the total mass fraction of Fe_3O_4/TAGA in the composites was 2.7 wt% (1.5/1.2 wt% Fe_3O_4/TAGA). The corresponding Fe_3O_4/TAGA/epoxy nanocomposites showed the highest EMI SE of 35 dB in the X-band. The significant improvement in SE was ascribed to the large conductive network formed, and the combination of dielectric and magnetic loss, leading to a superior impedance match. With the increase in the loading of NH_2–Fe_3O_4, SE_A was found to increase, suggesting that the addition of NH_2–Fe_3O_4 proved beneficial for shielding improvement contributed by magnetic loss. Fig. 11 shows the schematic for the fabrication of the Fe_3O_4/TAGA/epoxy nanocomposites.

Fe_3O_4@anisotropic reduced graphene oxide aerogel/epoxy (Fe_3O_4@AGA/EP) nanocomposites have been reported, where Fe_3O_4@AGA was prepared by hydrothermal reduction reaction, followed by unidirectional freezing approach.[105] Due to the synergistic effect arising from the magnetic and dielectric loss properties, the EMI SE of the Fe_3O_4@AGA/EP nanocomposites attained 40.4 dB along the radial direction when the mass ratio of Fe_3O_4 : GO was 2 : 1. In another study, to derive the

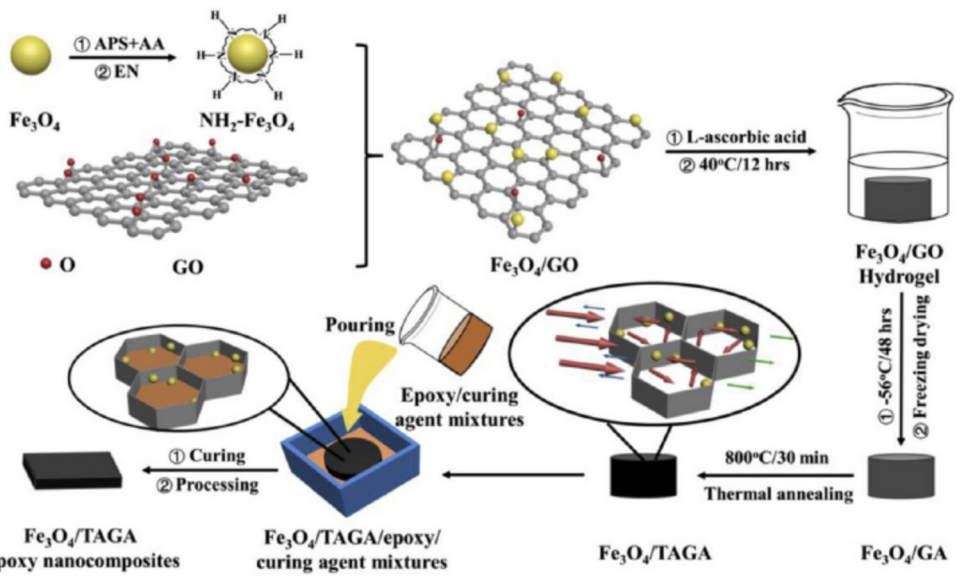

Fig. 11 The schematic for the fabrication of the Fe_3O_4/TAGA/epoxy nanocomposites; reproduced with permission from ref. 104, copyright reserved Elsevier 2019.

synergistic response, a unique structure was proposed by anchoring magnetic Fe_3O_4 nanoparticles onto the conductive 3D GF, and flexible PDMS composites were subsequently prepared.[106] The unique structure was realised by assembling CTAB-modified Fe_3O_4 and GF through mutual electrostatic interactions. The flexible composite has an advantage over the rigid one as it can be easily mounted on an irregular and curve structure. The EMI SE value of ~32.4 dB for the Fe_3O_4/GF/PDMS composite (~1.0 mm) was recorded in the frequency range of 8.2–12.4. The significant absorption contribution resulted from the synergy between GA, and the improved SE was attributed to the magnetic Fe_3O_4. Integration of 1D CNTs with 2D graphene to design a 3D continuous network has recently been performed to enrich the EMI SE.[107] The seminal improvement in SE further encouraged researchers to anchor magnetic particles on the 3D-CNTs skeletons, and to comprehend how this reasonably designed multiple structure played a role in improving the SE. A single integrated multi-phase hetero-nanostructure consisting of graphene, CNT and Fe_2O_3 (3D G–CNT–Fe_2O_3) was synthesized to fabricate the PEDOT:PSS/3D G–CNT–Fe_2O_3 composites film for EMI shielding application.[108] The 3D G–CNT–Fe_2O_3 nano-architecture was synthesized by a microwave irradiation method with ferrocene as an iron catalyst and carbon source for CNT growth on graphene. The flexible composite films were fabricated based on PEDOT:PSS, and various graphene-based fillers (such as 2D rGO, 2D G–Fe_2O_3, and 3D G–CNT–Fe_2O_3) were fabricated to ascertain the strong synergistic effect of 3D G–CNT–Fe_2O_3 on the EMI shielding properties of the films. The three-phase 3D G–CNT–Fe_2O_3 hetero-architecture showed improved reflection, absorption and scattering of EM radiation, which was ascribed to the strong synergy among 2D graphene, 1D CNT and 0D Fe_2O_3. The electrical conductivity values of PEDOT:PSS, 2DrGO/PEDOT:PSS, 2D G–Fe_2O_3/PEDOT:PSS, and 3D G–CNTFe_2O_3/PEDOT:PSS were found to be 15 400, 16 200, 17 400, and 22 800 S cm^{-1}, respectively. The EMI SE of the 2D rGO/PEDOT:PSS, 2D G–Fe_2O_3/PEDOT:PSS, and 3D G–CNTFe_2O_3/PEDOT:PSS composites films were found to be enhanced by 8%, 19%, and 25%, respectively. The remarkable improvement in SE was attributed to the excellent electrical conductivity of the multi-layered and interconnected nano-architecture, which assisted the easy delocalization of electric charges within the PEDOT:PSS network. Furthermore, iron particles induced a higher hysteresis and larger energy dissipation within the film. It is noteworthy that all the composite films exhibited an absorption-dominant mechanism rather than reflection, suggesting a synergistic contribution of the magnetic loss and dielectric loss. Fe_3O_4-decorated CNTs/rGO foam/epoxy (3D Fe_3O_4–CNTs/rGF/EP) nanocomposites with highly oriented 3D structures were fabricated by a facile template method.[109] The prepared composites with 0.24 wt% rGF and 2.76 wt% Fe_3O_4–CNTs resulted in a remarkable electrical conductivity of 15.3 S m^{-1} and EMI SE value of 36 dB within the X-band range. The synergistic response from the magnetic loss and efficient 3D framework structures was assumed as a reason behind such enhancement. The prominent interfacial contacts between CNTs, Fe_3O_4 and rGF resulted in an improved interfacial polarisation relaxation, leading to EM attenuation. From the absorption-dominant mechanism of the composites, it can be concurred that the introduction of Fe_3O_4 particles significantly

Table 3 Examples of 3D graphene/magnetic heterostructure polymer composites with their EMI SE attributes

Materials	Loading %	Preparation method	σ, S m^{-1}	EMI SE (dB)	Ref.
Fe_3O_4/GA/epoxy	Fe_3O_4 : GA 1.5 : 1.2	Template-casting	27.5	35	104
Fe_3O_4@GA/epoxy	2.1	Vacuum infiltration	32.1	40.4	105
Fe_3O_4/GF/PDMS	—	Dip coating	0.25	32.4	106
3D G-CNT-Fe_2O_3/PEDOT:PSS	0.28	Solution casting	228	130	108
Fe_3O_4-CNTs/rGF/epoxy	rGF : Fe_3O_4–CNTs 0.24 : 2.76	Template	15.3	36	109
rGO@FeNi/epoxy	2.1	Vacuum infiltration	38.7	46	33

Table 4 Comparison of the shielding performance of different 3D graphene scaffold-based composites with 2D graphene-based composites

3D graphene-based/polymer composites					2D graphene-based/polymer composites				
Material	Loading (%)	σ, S m^{-1}	EMI SE (dB)	Ref.	Material	Loading (%)	σ, S m^{-1}	EMI SE (dB)	Ref.
GA/EP	1	—	30	51	Graphene/EP	2.5	—	29	114
GA/PDMS	0.42	0.5	65	37	rGO/PU	2.5	—	53	115
3D graphene/MWCNTs/PDMS	0.98	100.99	56	90	Graphene-MWCNT/PU	10	—	47	116
Porous graphene/EP	1.59	318.48	38.78	77	rGO/PU	3.17	2.77	21.8	117
rGOs/AgNWs/PDMS	0.76	0.108	34.1	94	Graphene/SiCnW/PVDF	9.5	1.5	32.5	118
rGOs/AgPs/PDMS	0.76	45.3	58	92	GNP/Ni/PVDF	13	—	55.8	119
GF/PDMS	0.8		30	6	Graphene/WPU	5	43.6	38	120
GF/PDMS	3.07	103	54	76	GNS/TPU	0.12 (Vol)	35	14	121
GF/Silicon rubber	7	51.84	>20	78	rGO/PEI	2.5	—	22–26	122
GA/phenolic resin	0.33	73	35	72	GNP/PEK	5 (Vol)	2	33	123

promoted magnetic and dielectric losses. Amino-functionalized FeNi alloy particles (f-FeNi) have been loaded on the 3D GO regular honeycomb structure (GH) skeleton. This was followed by *in situ* reduction to prepare the rGH@FeNi aerogel, which was then impregnated by an epoxy resin following vacuum-assisted method to prepare the rGH@FeNi/epoxy composites for EMI shielding application.[33] The so-designed honeycomb conductive/magnetic structure expands the transmission path of the EM waves, leading to the increased attenuation of the EM waves by multiple reflections and scattering. Furthermore, the enhanced impedance matching between the rGH 3D conductive skeleton and epoxy resin matrix leads to increased hysteresis loss of the electromagnetic waves in the composites, which resulted in an SE value of 46 dB (Tables 3).

8. Conclusions and future direction

This article provides an overview of recent advancements in the design and fabrication of 3D graphene-based/polymer composites specifically for EMI shielding applications. The central focused has been on graphene foam and aerogels, along with the aerogel/dielectric/multiple heterostructure. The article also represents an analytical framework that could be employed to optimize the geometrical and structural parameters of the shield, and thereby tailor the impedance characteristics to achieve absorption-dominated shielding materials with diminished reflection. Contrary to thin film-based EMI shielding materials, a majority of the 3D graphene-based composites demonstrate an absorption-dominated shielding mechanism, which makes it more acceptable as the secondary pollution through reflection is minimal. However, few studies have been performed to decipher the influence of structural and geometrical factors on the shielding mechanism. A majority of the studies are based on trial-and-error methods without delving into the structure–EMI shielding property relationship. Structural and geometrical factors are crucial to tailor a surface impedance condition that is appropriate to achieve low reflection and high absorption. The design of a 3D structure does address the dispersion, agglomeration issue and impedance mismatch of graphene-based shielding to some extent. However, the concerns associated with the preparation of a scaffold are not yet regulated. The fabrication strategies currently in use lack overall competency to design a scaffold with different cellular morphologies (void fraction, density), and an ordered pore structure, and hence needs more optimisation and innovation. Employing more conducive processing techniques and strategies that could enable the pore size regulation, and designing scaffolds with different cellular morphologies are some of the areas of exploration that need urgent attention. A comparision of the EMI shielding performance between 2D graphene reinforced composites and the polymer composites reinforced by 3D graphene scaffold has been presented in Table 4.

Based on the available information, it can be conferred that the 3D graphene architectures shall accelerate the prospect towards the fabrication of high-performance absorption-dominated shielding materials. Although it will be too early to expect the engagement of these materials in industrial realm, the recent research activities nonetheless point towards a bright beginning. The crucial future directions that need to be undertaken for EMI shielding materials are as follows.

1. The current methods for designing 3D graphene scaffolds require innovative processing technologies that offer flexibility in regulating the pore size, creating ordered structures with aligned cell walls, customizing the cellular morphology to the desired scaffold properties, and controlling the thickness to achieve absorption-dominated shielding materials. Towards this, 3D printing technology holds the potential not only in providing freedom on the nanofiller proportion and size, but also renders the opportunity to design a scaffold having hierarchical pores that are apt for EM absorption. There have been a few reports on 3D printed graphene-based EMI shielding materials. For instance, Guo *et al.* reported on the shielding effectiveness value of 8.75 dB for a 3D printed lamellar graphene aerogel. Furthermore, a 3D printed lamellar Ti_3C_2Tx MXene/graphene hybrid aerogel has been reported by Hua *et al.*[110] However, the poor interlayer adhesion between the printed layers of the 3D printed scaffolds is an issue that needs to be studied with rigour. Furthermore, the development of polymer composites holding these 3D printed scaffolds requires more investigations to examine the feasibility of these structures.

2. An interesting strategy for fabricating 3D graphene-based aerogels and foams using the electrospinning technique has recently attracted much attention. These 3D structures, with their innovative architecture, have the potential to serve as EMI shields due to their creation of new interfaces and high porosity, which expand the paths for reflecting and scattering electromagnetic radiation. The known fabrication process includes precision electrospinning, self-assembly, multi-layer spinning, liquid/3D collectors, and processing into bulk aerogels and sponges.[111] Especially, precision electrospinning could be a potential technique to fabricate a highly porous 3D structure as it combines the additive manufacturing technique to exactly deposit the nanofiber in a predesigned pattern. A 3D macrostructure with heterointerfaces and excellent porosity has been prepared by assembling electrospun nanofibers. This process can be extended to prepare a graphene-based 3D structure, as well as through advanced formulation and optimization. Zheng *et al.* reported on an interfused core–shell heterogeneous reduced rGO/MXene aerogel (GMA) *via* coaxial wet spinning and freeze-drying, which exhibited an SE value of 83.3 dB that is supposedly higher than most of the carbon-based aerogels and foams.[112] Construction of Ti_3C_2Tx MXene@GO hybrid aerogel microspheres (M@GAMS) *via* electrostatic-spinning technique assisted by rapid freezing and freeze drying was also reported, and the study included the microwave absorption performance.[113] The design of 3D graphene aerogels and foams *via* electrospinning invoked exciting prospects. However, the issues concerning the mechanical stability is a big impediment. Studies covering the mechanical

robustness of such materials that are desirable for use in complex environments are scarce. Hence, it is premature to comment on the suitableness of such materials for EMI shielding applications. Furthermore, dispersing these 3D microscopic structures in a polymer matrix is another big challenge. As of now, not much progress has been made in this route.

3. The design of gradient-layered structures is a promising strategy to achieve low reflection and absorption-dominated EMI shielding. These structures consist of one or more absorption layers, which attenuates the EM radiation, and a reflection (shielding) layer, which reflects and attenuates the remaining EM radiation. The interface between the layers can produce substantial interfacial polarization that enhances attenuation *via* polarization loss. A few reports on a MXene-based layered composite foams EMI shielding material with an absorption-dominated mechanism are available. The strategy can be extended to 3D graphene-based polymer composites as well.

4. Considerable intervention in theoretical understanding is expected to build a consensus on the mechanism responsible for shielding, and to understand the *modus operandi* of different dimension particles, microstructural, and geometrical effects on the shielding performance. Therefore, more efforts in computational studies and analytical modeling are solicited to optimize the microstructural and geometrical aspects for achieving absorption-dominated shielding. Not only is a theoretical approach required to understand how the microstructures and geometry of the 3D skeleton enable the improvement in shielding effectiveness at a rudimentary level, but comprehending the interaction at the atomic level also could be relevant for devising suitable microstructure materials.

Author contributions

Conceptualization, S.C.; data curation, S.C.; writing—original draft preparation, S.C.; review and editing, T.K. All authors have read and agreed to the published version of the manuscript.

Conflicts of interest

The authors declare no conflict of interest.

Acknowledgements

S. C. thanks the Patent2Product fellowship through Office of Innovation and Commercialization University of Hawai'i system.

References

1 N. Bagotia, V. Choudhary and D. K. Sharma, Synergistic effect of graphene/multiwalled carbon nanotube hybrid fillers on mechanical, electrical and EMI shielding properties of polycarbonate/ethylene methyl acrylate nanocomposites, *Composites, Part B*, 2019, **159**, 378–388.
2 F. Ren, Z. Li, L. Xu, Z. Sun, P. Ren, D. Yan and Z. Li, Large-scale preparation of segregated PLA/carbon nanotube composite with high efficient electromagnetic interference shielding and favourable mechanical properties, *Composites, Part B*, 2018, **155**, 405–413.
3 S. Chhetri, N. C. Adak, P. Samanta, N. C. Murmu, S. K. Srivastava and T. Kuila, Synergistic effect of Fe3O4 anchored N-doped rGO hybrid on mechanical, thermal and electromagnetic shielding properties of epoxy composites, *Composites, Part B*, 2019, **166**, 371–381.
4 S. Umrao, T. K. Gupta, S. Kumar, V. K. Singh, M. K. Sultania, J. H. Jung, I.-K. Oh and A. Srivastava, Microwave-Assisted Synthesis of Boron and Nitrogen co-doped Reduced Graphene Oxide for the Protection of Electromagnetic Radiation in Ku-Band, *ACS Appl. Mater. Interfaces*, 2015, **7**, 19831–19842.
5 S. Chhetri, P. Samanta, N. Chandra Murmu, S. Kumar Srivastava and T. Kuila, Electromagnetic interference shielding and thermal properties of non-covalently functionalized reduced graphene oxide/epoxy composites, *AIMS Mater. Sci.*, 2016, **4**, 61–74.
6 Z. Chen, C. Xu, C. Ma, W. Ren and H.-M. Cheng, Lightweight and Flexible Graphene Foam Composites for High-Performance Electromagnetic Interference Shielding, *Adv. Mater.*, 2013, **25**, 1296–1300.
7 M. R. Tofighi, *Interaction between electromagnetic waves and biological materials*, ed. C. Li, M. Tofighi, D. Schreurs and T-Z. J. Horng, Principles and Applications of RF/Microwave in Healthcare and Biosensing. Elsevier, 2017, pp. 53-101.
8 J. Srivastava, P. Kumar Khanna, P. V. More and N. Singh, Chemically Synthesized Ag/PPy-PVA Polymer Nanocomposite Films As Potential EMI Shielding Material In X-band, *Adv. Mater. Lett.*, 2017, **8**, 42–48.
9 B. P. Singh, Prasanta, V. Choudhary, P. Saini, S. Pande, V. N. Singh and R. B. Mathur, Enhanced microwave shielding and mechanical properties of high loading MWCNT–epoxy composites, *J. Nanopart. Res.*, 2013, **15**, 1554.
10 H. Abbasi, M. Antunes and J. I. Velasco, Recent advances in carbon-based polymer nanocomposites for electromagnetic interference shielding, *Prog. Mater. Sci.*, 2019, **103**, 319–373.
11 R. Kumar, D. P. Mondal, A. Chaudhary, M. Shafeeq and S. Kumari, Excellent EMI shielding performance and thermal insulating properties in lightweight, multifunctional carbon-cenosphere composite foams, *Composites, Part A*, 2018, **112**, 475–484.
12 S. K. Srivastava and K. Manna, Recent advancements in the electromagnetic interference shielding performance of nanostructured materials and their nanocomposites: a review, *J. Mater. Chem. A*, 2022, **10**, 7431–7496.
13 P. Kathirgamanathan, Novel cable shielding materials based on the impregnation of microporous membranes

with inherently conducting polymers, *Adv. Mater.*, 1993, **5**, 281–283.

14 P. Li, D. Du, L. Guo, Y. Guo and J. Ouyang, Stretchable and conductive polymer films for high-performance electromagnetic interference shielding, *J. Mater. Chem. C*, 2016, **4**, 6525–6532.

15 Y. Yang, M. C. Gupta, K. L. Dudley and R. W. Lawrence, Conductive Carbon Nanofiber-Polymer Foam Structures, *Adv. Mater.*, 2005, **17**, 1999–2003.

16 L. Zhang, L. B. Wang, K. Y. See and J. Ma, Effect of carbon nanofiber reinforcement on electromagnetic interference shielding effectiveness of syntactic foam, *J. Mater. Sci.*, 2013, **48**, 7757–7763.

17 Y. Yang, M. C. Gupta, K. L. Dudley and R. W. Lawrence, Novel Carbon Nanotube–Polystyrene Foam Composites for Electromagnetic Interference Shielding, *Nano Lett.*, 2005, **5**, 2131–2134.

18 J. Liang, Y. Wang, Y. Huang, Y. Ma, Z. Liu, J. Cai, C. Zhang, H. Gao and Y. Chen, Electromagnetic interference shielding of graphene/epoxy composites, *Carbon*, 2009, **47**, 922–925.

19 R. Bera, S. Suin, S. Maiti, N. K. Shrivastava and B. B. Khatua, Carbon nanohorn and graphene nanoplate based polystyrene nanocomposites for superior electromagnetic interference shielding applications, *J. Appl. Polym. Sci.*, 2015, **132**, 42803.

20 S. Chhetri, T. Kuila and N. C. Murmu, in *Graphene Technology: From Laboratory to Fabrication*, ed. S. Nazarpour and S. R. Waite, Wiley-VCH Verlag GmbH & Co. KGaA, Weinheim, Germany, 2016, pp. 63–111.

21 Z. Dang, M. Zheng and J. Zha, 1D/2D Carbon Nanomaterial–Polymer Dielectric Composites with High Permittivity for Power Energy Storage Applications, *Small*, 2016, **12**, 1688–1701.

22 M. Panahi-Sarmad, M. Noroozi, X. Xiao and C. B. Park, Recent Advances in Graphene-Based Polymer Nanocomposites and Foams for Electromagnetic Interference Shielding Applications, *Ind. Eng. Chem. Res.*, 2022, **61**, 1545–1568.

23 Y. Xia, W. Gao and C. Gao, A Review on Graphene–Based Electromagnetic Functional Materials: Electromagnetic Wave Shielding and Absorption, *Adv. Funct. Mater.*, 2022, **32**, 2204591.

24 Q. Song, F. Ye, L. Kong, Q. Shen, L. Han, L. Feng, G. Yu, Y. Pan and H. Li, Graphene and MXene Nanomaterials: Toward High–Performance Electromagnetic Wave Absorption in Gigahertz Band Range, *Adv. Funct. Mater.*, 2020, **30**, 2000475.

25 P. Song, B. Liu, C. Liang, K. Ruan, H. Qiu, Z. Ma, Y. Guo and J. Gu, Lightweight, Flexible Cellulose-Derived Carbon Aerogel@Reduced Graphene Oxide/PDMS Composites with Outstanding EMI Shielding Performances and Excellent Thermal Conductivities, *Nano-Micro Lett.*, 2021, **13**, 91.

26 B. Zhao, M. Hamidinejad, S. Wang, P. Bai, R. Che, R. Zhang and C. B. Park, Advances in electromagnetic shielding properties of composite foams, *J. Mater. Chem. A*, 2021, **9**, 8896–8949.

27 D. Tian, Y. Xu, Y. Wang, Z. Lei, Z. Lin, T. Zhao, Y. Hu, R. Sun and C.-P. Wong, In situ metallized carbon nanotubes/poly(styrene-butadiene-styrene) (CNTs/SBS) foam for electromagnetic interference shielding, *Chem. Eng. J.*, 2021, **420**, 130482.

28 G. Weng, J. Li, M. Alhabeb, C. Karpovich, H. Wang, J. Lipton, K. Maleski, J. Kong, E. Shaulsky, M. Elimelech, Y. Gogotsi and A. D. Taylor, Layer–by–Layer Assembly of Cross–Functional Semi–transparent MXene–Carbon Nanotubes Composite Films for Next–Generation Electromagnetic Interference Shielding, *Adv. Funct. Mater.*, 2018, **28**, 1803360.

29 X. Jia, Y. Li, B. Shen and W. Zheng, Evaluation, fabrication and dynamic performance regulation of green EMI-shielding materials with low reflectivity: A review, *Composites, Part B*, 2022, **233**, 109652.

30 S. H. Ryu, Y. K. Han, S. J. Kwon, T. Kim, B. M. Jung, S.-B. Lee and B. Park, Absorption-dominant, low reflection EMI shielding materials with integrated metal mesh/TPU/CIP composite, *Chem. Eng. J.*, 2022, **428**, 131167.

31 M. Hamidinejad, M. Salari, L. Ma, N. Moghimian, B. Zhao, H. K. Taylor, T. Filleter and C. B. Park, Electrically and thermally graded microcellular polymer/graphene nanoplatelet composite foams and their EMI shielding properties, *Carbon*, 2022, **187**, 153–164.

32 L. Wang, Y. Wu, Y. Wang, H. Li, N. Jiang and K. Niu, Laterally compressed graphene foam/acrylonitrile butadiene styrene composites for electromagnetic interference shielding, *Composites, Part A*, 2020, **133**, 105887.

33 P. Song, Z. Ma, H. Qiu, Y. Ru and J. Gu, High-Efficiency Electromagnetic Interference Shielding of rGO@FeNi/Epoxy Composites with Regular Honeycomb Structures, *Nano-Micro Lett.*, 2022, **14**, 51.

34 A. Idowu, B. Boesl and A. Agarwal, 3D graphene foam-reinforced polymer composites – A review, *Carbon*, 2018, **135**, 52–71.

35 H. Liu, Y. Xu, X. Zhao, D. Han, F. Zhao and Q. Yang, Lightweight leaf-structured carbon nanotubes/graphene foam and the composites with polydimethylsiloxane for electromagnetic interference shielding, *Carbon*, 2022, **191**, 183–194.

36 E. Choi, J. Lee, Y.-J. Kim, H. Kim, M. Kim, J. Hong, Y. C. Kang, C. M. Koo, D. W. Kim and S. J. Kim, Enhanced stability of Ti3C2Tx MXene enabled by continuous ZIF-8 coating, *Carbon*, 2022, **191**, 593–599.

37 W. Gao, N. Zhao, T. Yu, J. Xi, A. Mao, M. Yuan, H. Bai and C. Gao, High-efficiency electromagnetic interference shielding realized in nacre-mimetic graphene/polymer composite with extremely low graphene loading, *Carbon*, 2020, **157**, 570–577.

38 H. Liu, Y. Xu, H. Yong, Y. Huang, D. Han, K. Yang and Q. Yang, Studies on electromagnetic interference shielding effect mechanisms of leaf-like three-dimensional carbon nanotubes/graphene aerogel film and the compo-

sites with polydimethylsiloxane, *Carbon*, 2023, **207**, 261–269.
39 L. Ma, M. Hamidinejad, L. Wei, B. Zhao and C. B. Park, Absorption-dominant EMI shielding polymer composite foams: Microstructure and geometry optimization, *Mater. Today Phys.*, 2023, **30**, 100940.
40 L. Ma, L. Wei, M. Hamidinejad and C. B. Park, Layered polymer composite foams for broadband ultra-low reflectance EMI shielding: a computationally guided fabrication approach, *Mater. Horiz.*, 2023, **10**, 4423–4437.
41 D. R. Jackson, in *The Electrical Engineering Handbook*, Elsevier, 2005, pp. 513–524.
42 R. F. Harrington, *Time-Harmonic Electromagnetic Fields*, IEEE, 2001.
43 S. M. Yang, Y. Y. Chang, Y. C. Hsieh and Y. J. Lee, Electromagnetic shielding effectiveness of multilayer metallic thin film on plastic substrates, *J. Appl. Polym. Sci.*, 2008, **110**, 1403–1410.
44 L. Wei, J. Ma, L. Ma, C. Zhao, M. Xu, Q. Qi, W. Zhang, L. Zhang, X. He and C. B. Park, Computational Optimizing the Electromagnetic Wave Reflectivity of Double–Layered Polymer Nanocomposites, *Small Methods*, 2022, **6**, 2101510.
45 T. J. Rouphael, in *Wireless Receiver Architectures and Design*, Elsevier, 2014, pp. 1–60.
46 J. Semmlow, in *Circuits, Signals and Systems for Bioengineers*, Elsevier, 2018, pp. 631–679.
47 T. Khongdeach, W. Chongburee and N. Homsup, Determination of power line transfer functions by a method of impedance transfer and voltage spread, *Prog. Electromagn. Res.*, 2018, **71**, 63–74.
48 L. Ma, M. Hamidinejad, C. Liang, B. Zhao, S. Habibpour, A. Yu, T. Filleter and C. B. Park, Enhanced electromagnetic wave absorption performance of polymer/SiC-nanowire/MXene (Ti3C2Tx) composites, *Carbon*, 2021, **179**, 408–416.
49 B. Zhao, X. Guo, W. Zhao, J. Deng, B. Fan, G. Shao, Z. Bai and R. Zhang, Facile synthesis of yolk–shell Ni@void@SnO2(Ni3Sn2) ternary composites via galvanic replacement/Kirkendall effect and their enhanced microwave absorption properties, *Nano Res.*, 2017, **10**, 331–343.
50 X. Huang, G. Yu, Y. Zhang, M. Zhang and G. Shao, Design of cellular structure of graphene aerogels for electromagnetic wave absorption, *Chem. Eng. J.*, 2021, **426**, 131894.
51 Y.-J. Wan, S.-H. Yu, W.-H. Yang, P.-L. Zhu, R. Sun, C.-P. Wong and W.-H. Liao, Tuneable cellular-structured 3D graphene aerogel and its effect on electromagnetic interference shielding performance and mechanical properties of epoxy composites, *RSC Adv.*, 2016, **6**, 56589–56598.
52 Z. Chen, W. Ren, L. Gao, B. Liu, S. Pei and H.-M. Cheng, Three-dimensional flexible and conductive interconnected graphene networks grown by chemical vapour deposition, *Nat. Mater.*, 2011, **10**, 424–428.
53 X. Xiao, T. E. Beechem, M. T. Brumbach, T. N. Lambert, D. J. Davis, J. R. Michael, C. M. Washburn, J. Wang, S. M. Brozik, D. R. Wheeler, D. B. Burckel and R. Polsky, Lithographically Defined Three-Dimensional Graphene Structures, *ACS Nano*, 2012, **6**, 3573–3579.
54 Z. Bo, K. Yu, G. Lu, P. Wang, S. Mao and J. Chen, Understanding growth of carbon nanowalls at atmospheric pressure using normal glow discharge plasma-enhanced chemical vapor deposition, *Carbon*, 2011, **49**, 1849–1858.
55 Y. Ma and Y. Chen, Three-dimensional graphene networks: synthesis, properties and applications, *Natl. Sci. Rev.*, 2015, **2**, 40–53.
56 X. Cao, Z. Yin and H. Zhang, Three-dimensional graphene materials: preparation, structures and application in supercapacitors, *Energy Environ. Sci.*, 2014, **7**, 1850–1865.
57 S. Nardecchia, D. Carriazo, M. L. Ferrer, M. C. Gutiérrez and F. Del Monte, Three dimensional macroporous architectures and aerogels built of carbon nanotubes and/or graphene: synthesis and applications, *Chem. Soc. Rev.*, 2013, **42**, 794–830.
58 H. Bi, X. Xie, K. Yin, Y. Zhou, S. Wan, L. He, F. Xu, F. Banhart, L. Sun and R. S. Ruoff, Spongy Graphene as a Highly Efficient and Recyclable Sorbent for Oils and Organic Solvents, *Adv. Funct. Mater.*, 2012, **22**, 4421–4425.
59 Z. Tang, S. Shen, J. Zhuang and X. Wang, Noble-Metal-Promoted Three-Dimensional Macroassembly of Single-Layered Graphene Oxide, *Angew. Chem., Int. Ed.*, 2010, **49**, 4603–4607.
60 Y. Li, K. Sheng, W. Yuan and G. Shi, A high-performance flexible fibre-shaped electrochemical capacitor based on electrochemically reduced graphene oxide, *Chem. Commun.*, 2013, **49**, 291–293.
61 H. Huang, P. Chen, X. Zhang, Y. Lu and W. Zhan, Edge-to-Edge Assembled Graphene Oxide Aerogels with Outstanding Mechanical Performance and Superhigh Chemical Activity, *Small*, 2013, **9**, 1397–1404.
62 Y. Xu, X. Huang, Z. Lin, X. Zhong, Y. Huang and X. Duan, One-step strategy to graphene/Ni(OH)2 composite hydrogels as advanced three-dimensional supercapacitor electrode materials, *Nano Res.*, 2013, **6**, 65–76.
63 Y. Li, W. Cui, L. Liu, R. Zong, W. Yao, Y. Liang and Y. Zhu, Removal of Cr(VI) by 3D TiO 2 -graphene hydrogel via adsorption enriched with photocatalytic reduction, *Appl. Catal., B*, 2016, **199**, 412–423.
64 Z. Cheng, R. Wang, Y. Wang, Y. Cao, Y. Shen, Y. Huang and Y. Chen, Recent advances in graphene aerogels as absorption-dominated electromagnetic interference shielding materials, *Carbon*, 2023, **205**, 112–137.
65 Y. Wei, L. Xu, K. Yang, Y. Wang, Z. Wang, Y. Kong and H. Xue, Electrosorption of Toxic Heavy Metal Ions by Mono S- or N-Doped and S, N-Codoped 3D Graphene Aerogels, *J. Electrochem. Soc.*, 2017, **164**, E17–E22.
66 P. Liu, X. Li, X. Chang, P. Min, C. Shu, Y. Li, Y. Kang and Z.-Z. Yu, Highly anisotropic graphene aerogels fabricated by calcium ion-assisted unidirectional freezing for highly sensitive sensors and efficient cleanup of crude oil spills, *Carbon*, 2021, **178**, 301–309.

67 Z. Jia, M. Zhang, B. Liu, F. Wang, G. Wei and Z. Su, Graphene Foams for Electromagnetic Interference Shielding: A Review, *ACS Appl. Nano Mater.*, 2020, **3**, 6140–6155.
68 Z. Wang, X. Shen, M. A. Garakani, X. Lin, Y. Wu, X. Liu, X. Sun and J.-K. Kim, Graphene Aerogel/Epoxy Composites with Exceptional Anisotropic Structure and Properties, *ACS Appl. Mater. Interfaces*, 2015, **7**, 5538–5549.
69 Y.-Y. Wang, F. Zhang, N. Li, J.-F. Shi, L.-C. Jia, D.-X. Yan and Z.-M. Li, Carbon-based aerogels and foams for electromagnetic interference shielding: A review, *Carbon*, 2023, **205**, 10–26.
70 X.-H. Li, X. Li, K.-N. Liao, P. Min, T. Liu, A. Dasari and Z.-Z. Yu, Thermally Annealed Anisotropic Graphene Aerogels and Their Electrically Conductive Epoxy Composites with Excellent Electromagnetic Interference Shielding Efficiencies, *ACS Appl. Mater. Interfaces*, 2016, **8**, 33230–33239.
71 P. Song, C. Liang, L. Wang, H. Qiu, H. Gu, J. Kong and J. Gu, Obviously improved electromagnetic interference shielding performances for epoxy composites via constructing honeycomb structural reduced graphene oxide, *Compos. Sci. Technol.*, 2019, **181**, 107698.
72 Y. Chen, H.-B. Zhang, M. Wang, X. Qian, A. Dasari and Z.-Z. Yu, Phenolic resin-enhanced three-dimensional graphene aerogels and their epoxy nanocomposites with high mechanical and electromagnetic interference shielding performances, *Compos. Sci. Technol.*, 2017, **152**, 254–262.
73 D. Han, Y.-H. Zhao, S.-L. Bai and W. C. Ping, High shielding effectiveness of multilayer graphene oxide aerogel film/polymer composites, *RSC Adv.*, 2016, **6**, 92168–92174.
74 Y. Huangfu, K. Ruan, H. Qiu, Y. Lu, C. Liang, J. Kong and J. Gu, Fabrication and investigation on the PANI/MWCNT/thermally annealed graphene aerogel/epoxy electromagnetic interference shielding nanocomposites, *Composites, Part A*, 2019, **121**, 265–272.
75 X. Yang, S. Fan, Y. Li, Y. Guo, Y. Li, K. Ruan, S. Zhang, J. Zhang, J. Kong and J. Gu, Synchronously improved electromagnetic interference shielding and thermal conductivity for epoxy nanocomposites by constructing 3D copper nanowires/thermally annealed graphene aerogel framework, *Composites, Part A*, 2020, **128**, 105670.
76 F. Xu, R. Chen, Z. Lin, Y. Qin, Y. Yuan, Y. Li, X. Zhao, M. Yang, X. Sun, S. Wang, Q. Peng, Y. Li and X. He, Superflexible Interconnected Graphene Network Nanocomposites for High-Performance Electromagnetic Interference Shielding, *ACS Omega*, 2018, **3**, 3599–3607.
77 K. Ba, M. Zhang, X. Wang, P. Xu, W. Song, C. Wang, W. Yang and Y. Liu, Porous graphene composites fabricated by template method used for electromagnetic shielding and thermal conduction, *Diamond Relat. Mater.*, 2023, **131**, 109585.
78 B. Fan, L. Xing, K. Yang, Y. Yang, F. Zhou, G. Tong and W. Wu, Salt-templated graphene nanosheet foams filled in silicon rubber toward prominent EMI shielding effectiveness and high thermal conductivity, *Carbon*, 2023, **207**, 317–327.
79 L. Wang, H. Li, S. Xiao, M. Zhu and J. Yang, Preparation of p-Phenylenediamine Modified Graphene Foam/Polyaniline@Epoxy Composite with Superior Thermal and EMI Shielding Performance, *Polymers*, 2021, **13**, 2324.
80 Y. Wu, Z. Wang, X. Liu, X. Shen, Q. Zheng, Q. Xue and J.-K. Kim, Ultralight Graphene Foam/Conductive Polymer Composites for Exceptional Electromagnetic Interference Shielding, *ACS Appl. Mater. Interfaces*, 2017, **9**, 9059–9069.
81 C. Wang, X. Han, P. Xu, X. Zhang, Y. Du, S. Hu, J. Wang and X. Wang, The electromagnetic property of chemically reduced graphene oxide and its application as microwave absorbing material, *Appl. Phys. Lett.*, 2011, **98**, 072906.
82 R. C. Che, L.-M. Peng, X. F. Duan, Q. Chen and X. L. Liang, Microwave Absorption Enhancement and Complex Permittivity and Permeability of Fe Encapsulated within Carbon Nanotubes, *Adv. Mater.*, 2004, **16**, 401–405.
83 C. Liang, H. Qiu, Y. Han, H. Gu, P. Song, L. Wang, J. Kong, D. Cao and J. Gu, Superior electromagnetic interference shielding 3D graphene nanoplatelets/reduced graphene oxide foam/epoxy nanocomposites with high thermal conductivity, *J. Mater. Chem. C*, 2019, **7**, 2725–2733.
84 L. Han, K. Li, Y. Fu, X. Yin, Y. Jiao and Q. Song, Multifunctional electromagnetic interference shielding 3D reduced graphene oxide/vertical edge-rich graphene/epoxy nanocomposites with remarkable thermal management performance, *Compos. Sci. Technol.*, 2022, **222**, 109407.
85 J. Li, X. Zhao, W. Wu, X. Ji, Y. Lu and L. Zhang, Bubble-templated rGO-graphene nanoplatelet foams encapsulated in silicon rubber for electromagnetic interference shielding and high thermal conductivity, *Chem. Eng. J.*, 2021, **415**, 129054.
86 S. Anand, M. C. Vu, D. Mani, J.-B. Kim, T.-H. Jeong, Md. A. Islam and S.-R. Kim, Dual 3D networks of graphene derivatives based polydimethylsiloxane composites for electrical insulating electronic packaging materials with outstanding electromagnetic interference shielding and thermal dissipation performances, *Chem. Eng. J.*, 2023, **462**, 142017.
87 S. Zhao, Y. Yan, A. Gao, S. Zhao, J. Cui and G. Zhang, Flexible Polydimethylsilane Nanocomposites Enhanced with a Three-Dimensional Graphene/Carbon Nanotube Bicontinuous Framework for High-Performance Electromagnetic Interference Shielding, *ACS Appl. Mater. Interfaces*, 2018, **10**, 26723–26732.
88 X. Sun, X. Liu, X. Shen, Y. Wu, Z. Wang and J.-K. Kim, Graphene foam/carbon nanotube/poly(dimethyl siloxane) composites for exceptional microwave shielding, *Composites, Part A*, 2016, **85**, 199–206.
89 S. Zhu, C. Xing, F. Wu, X. Zuo, Y. Zhang, C. Yu, M. Chen, W. Li, Q. Li and L. Liu, Cake-like flexible carbon nanotubes/graphene composite prepared via a facile method for high-performance electromagnetic interference shielding, *Carbon*, 2019, **145**, 259–265.
90 H. Jia, Q.-Q. Kong, Z. Liu, X.-X. Wei, X.-M. Li, J.-P. Chen, F. Li, X. Yang, G.-H. Sun and C.-M. Chen, 3D graphene/

carbon nanotubes/polydimethylsiloxane composites as high-performance electromagnetic shielding material in X-band, *Composites, Part A*, 2020, **129**, 105712.

91 Z. Ma, A. Wei, J. Ma, L. Shao, H. Jiang, D. Dong, Z. Ji, Q. Wang and S. Kang, Lightweight, compressible and electrically conductive polyurethane sponges coated with synergistic multiwalled carbon nanotubes and graphene for piezoresistive sensors, *Nanoscale*, 2018, **10**, 7116–7126.

92 C. Liang, P. Song, H. Qiu, Y. Zhang, X. Ma, F. Qi, H. Gu, J. Kong, D. Cao and J. Gu, Constructing interconnected spherical hollow conductive networks in silver platelets/reduced graphene oxide foam/epoxy nanocomposites for superior electromagnetic interference shielding effectiveness, *Nanoscale*, 2019, **11**, 22590–22598.

93 R. Kumaran, A. V. Kumar, S. Ramaprabhu and V. Subramanian, Absorption-enhanced EMI shielding using silver decorated three-dimensional porous architected reduced graphene oxide in polybenzoxazine composites, *New J. Chem.*, 2021, **45**, 16939–16948.

94 Y. Li, C. Li, S. Zhao, J. Cui, G. Zhang, A. Gao and Y. Yan, Facile fabrication of highly conductive and robust three-dimensional graphene/silver nanowires bicontinuous skeletons for electromagnetic interference shielding silicone rubber nanocomposites, *Composites, Part A*, 2019, **119**, 101–110.

95 L. Kong, X. Yin, M. Han, X. Yuan, Z. Hou, F. Ye, L. Zhang, L. Cheng, Z. Xu and J. Huang, Macroscopic bioinspired graphene sponge modified with in situ grown carbon nanowires and its electromagnetic properties, *Carbon*, 2017, **111**, 94–102.

96 X. Fan, Q. Gao, Y. Zhang, J. Qin, Y. Zhao, X. Shi and G. Zhang, Anisotropic microcellular epoxy/rGO-SCF aerogel foam with excellent compressibility and superior electromagnetic interference shielding performance, *Compos. Sci. Technol.*, 2022, **230**, 109718.

97 X. Zeng, X. Cheng, R. Yu and G. D. Stucky, Electromagnetic microwave absorption theory and recent achievements in microwave absorbers, *Carbon*, 2020, **168**, 606–623.

98 J. Xu, R. Shu, Z. Wan and J. Shi, Construction of three-dimensional hierarchical porous nitrogen-doped reduced graphene oxide/hollow cobalt ferrite composite aerogels toward highly efficient electromagnetic wave absorption, *J. Mater. Sci. Technol.*, 2023, **132**, 193–200.

99 W.-L. Song, X.-T. Guan, L.-Z. Fan, W.-Q. Cao, C.-Y. Wang, Q.-L. Zhao and M.-S. Cao, Magnetic and conductive graphene papers toward thin layers of effective electromagnetic shielding, *J. Mater. Chem. A*, 2015, **3**, 2097–2107.

100 M.-S. Cao, J. Yang, W.-L. Song, D.-Q. Zhang, B. Wen, H.-B. Jin, Z.-L. Hou and J. Yuan, Ferroferric Oxide/Multiwalled Carbon Nanotube vs Polyaniline/Ferroferric Oxide/Multiwalled Carbon Nanotube Multiheterostructures for Highly Effective Microwave Absorption, *ACS Appl. Mater. Interfaces*, 2012, **4**, 6949–6956.

101 Y.-H. Chen, Z.-H. Huang, M.-M. Lu, W.-Q. Cao, J. Yuan, D.-Q. Zhang and M.-S. Cao, 3D Fe_3O_4 nanocrystals decorating carbon nanotubes to tune electromagnetic properties and enhance microwave absorption capacity, *J. Mater. Chem. A*, 2015, **3**, 12621–12625.

102 M.-M. Lu, M.-S. Cao, Y.-H. Chen, W.-Q. Cao, J. Liu, H.-L. Shi, D.-Q. Zhang, W.-Z. Wang and J. Yuan, Multiscale Assembly of Grape-Like Ferroferric Oxide and Carbon Nanotubes: A Smart Absorber Prototype Varying Temperature to Tune Intensities, *ACS Appl. Mater. Interfaces*, 2015, **7**, 19408–19415.

103 H. Chen, W. Ma, Z. Huang, Y. Zhang, Y. Huang and Y. Chen, Graphene–Based Materials toward Microwave and Terahertz Absorbing Stealth Technologies, *Adv. Opt. Mater.*, 2019, **7**, 1801318.

104 Y. Huangfu, C. Liang, Y. Han, H. Qiu, P. Song, L. Wang, J. Kong and J. Gu, Fabrication and investigation on the Fe3O4/thermally annealed graphene aerogel/epoxy electromagnetic interference shielding nanocomposites, *Compos. Sci. Technol.*, 2019, **169**, 70–75.

105 X. Yang, Y. Zhang, J. Luo, R. Tusiime, C. Lu, Y. Xue, J. Zhou, Y. Liu, H. Zhang and J. Yu, Fe3O4 uniformly decorated reduced graphene oxide aerogel for epoxy nanocomposites with high EMI shielding performance, *Compos. Commun.*, 2022, **36**, 101391.

106 S. Zhu, Q. Cheng, C. Yu, X. Pan, X. Zuo, J. Liu, M. Chen, W. Li, Q. Li and L. Liu, Flexible Fe3O4/graphene foam/poly dimethylsiloxane composite for high-performance electromagnetic interference shielding, *Compos. Sci. Technol.*, 2020, **189**, 108012.

107 Q. Song, F. Ye, X. Yin, W. Li, H. Li, Y. Liu, K. Li, K. Xie, X. Li, Q. Fu, L. Cheng, L. Zhang and B. Wei, Carbon Nanotube–Multilayered Graphene Edge Plane Core–Shell Hybrid Foams for Ultrahigh–Performance Electromagnetic–Interference Shielding, *Adv. Mater.*, 2017, **29**, 1701583.

108 S.-H. Lee, D. Kang and I.-K. Oh, Multilayered graphene-carbon nanotube-iron oxide three-dimensional heterostructure for flexible electromagnetic interference shielding film, *Carbon*, 2017, **111**, 248–257.

109 C. Liang, P. Song, A. Ma, X. Shi, H. Gu, L. Wang, H. Qiu, J. Kong and J. Gu, Highly oriented three-dimensional structures of Fe3O4 decorated CNTs/reduced graphene oxide foam/epoxy nanocomposites against electromagnetic pollution, *Compos. Sci. Technol.*, 2019, **181**, 107683.

110 H. Guo, T. Hua, J. Qin, Q. Wu, R. Wang, B. Qian, L. Li and X. Shi, A New Strategy of 3D Printing Lightweight Lamellar Graphene Aerogels for Electromagnetic Interference Shielding and Piezoresistive Sensor Applications, *Adv. Mater. Technol.*, 2022, **7**, 2101699.

111 J. K. Y. Lee, N. Chen, S. Peng, L. Li, L. Tian, N. Thakor and S. Ramakrishna, Polymer-based composites by electrospinning: Preparation & functionalization with nanocarbons, *Prog. Polym. Sci.*, 2018, **86**, 40–84.

112 X. Zheng, J. Tang, P. Wang, Z. Wang, L. Zou and C. Li, Interfused core-shell heterogeneous graphene/MXene fiber aerogel for high-performance and durable electromagnetic interference shielding, *J. Colloid Interface Sci.*, 2022, **628**, 994–1003.

113 Y. Li, F. Meng, Y. Mei, H. Wang, Y. Guo, Y. Wang, F. Peng, F. Huang and Z. Zhou, Electrospun generation of Ti3C2Tx MXene@graphene oxide hybrid aerogel microspheres for tunable high-performance microwave absorption, *Chem. Eng. J.*, 2020, **391**, 123512.

114 B. V. S. R. N. Santhosi, K. Ramji and N. B. R. M. Rao, Design and development of polymeric nanocomposite reinforced with graphene for effective EMI shielding in X-band, *Phys. B*, 2020, **586**, 412144.

115 M. Zahid, Y. Nawab, N. Gulzar, Z. A. Rehan, M. F. Shakir, A. Afzal, I. A. Rashid and A. Tariq, Fabrication of reduced graphene oxide (RGO) and nanocomposite with thermoplastic polyurethane (TPU) for EMI shielding application, *J. Mater. Sci.: Mater. Electron.*, 2020, **31**, 967–974.

116 M. Verma, S. S. Chauhan, S. K. Dhawan and V. Choudhary, Graphene nanoplatelets/carbon nanotubes/polyurethane composites as efficient shield against electromagnetic polluting radiations, *Composites, Part B*, 2017, **120**, 118–127.

117 Q. Jiang, X. Liao, J. Li, J. Chen, G. Wang, J. Yi, Q. Yang and G. Li, Flexible thermoplastic polyurethane/reduced graphene oxide composite foams for electromagnetic interference shielding with high absorption characteristic, *Composites, Part A*, 2019, **123**, 310–319.

118 C. Liang, M. Hamidinejad, L. Ma, Z. Wang and C. B. Park, Lightweight and flexible graphene/SiC-nanowires/poly (vinylidene fluoride) composites for electromagnetic interference shielding and thermal management, *Carbon*, 2020, **156**, 58–66.

119 B. Zhao, S. Wang, C. Zhao, R. Li, S. M. Hamidinejad, Y. Kazemi and C. B. Park, Synergism between carbon materials and Ni chains in flexible poly(vinylidene fluoride) composite films with high heat dissipation to improve electromagnetic shielding properties, *Carbon*, 2018, **127**, 469–478.

120 S.-T. Hsiao, C.-C. M. Ma, H.-W. Tien, W.-H. Liao, Y.-S. Wang, S.-M. Li, C.-Y. Yang, S.-C. Lin and R.-B. Yang, Effect of Covalent Modification of Graphene Nanosheets on the Electrical Property and Electromagnetic Interference Shielding Performance of a Water-Borne Polyurethane Composite, *ACS Appl. Mater. Interfaces*, 2015, **7**, 2817–2826.

121 R. Jan, A. Habib, M. A. Akram, I. Ahmad, A. Shah, M. Sadiq and A. Hussain, Flexible, thin films of graphene–polymer composites for EMI shielding, *Mater. Res. Express*, 2017, **4**, 035605.

122 P. Sawai, P. P. Chattopadhaya and S. Banerjee, Synthesized reduce Graphene Oxide (rGO) filled Polyetherimide based nanocomposites for EMI Shielding applications, *Mater. Today: Proc.*, 2018, **5**, 9989–9999.

123 S. D. Bhosale, S. D. Gaikwad, R. D. Gadve and R. K. Goyal, Synergistic effects of graphene nanoplatelets on X-band electromagnetic interference shielding, thermal expansion and thermal stability of poly(ether-ketone) based nanocomposites, *Mater. Sci. Eng., B*, 2021, **265**, 115038.